INRIA

INSTITUT NATIONAL DE RECHERCHE EN INFORMATIQUE ET EN AUTOMATIQUE

Simulations of MHD flows with moving interfaces

Jean-Frédéric Gerbeau — Claude Le Bris — Tony Lelièvre

N° 4277

Octobre 2001

THÈME 4

ISSN 0249-6399 ISRN INRIA/RR--4277--FR+ENG

INRIA
ROCQUENCOURT

Simulations of MHD flows with moving interfaces

Jean-Frédéric Gerbeau* , Claude Le Bris † , Tony Lelièvre†

Thème 4 — Simulation et optimisation
de systèmes complexes
Projet M3N

Rapport de recherche n° 4277 — Octobre 2001 — 37 pages

Abstract: We report on the numerical simulation of a two-fluid magnetohydrodynamics problem arising in the industrial production of aluminium. The motion of the two non miscible fluids is modeled through the incompressible Navier-Stokes equations coupled with the Maxwell equations. An Arbitrary Lagrangian Eulerian formulation is used to take into account the motion of the interface separating the two fuids. Details on the numerical analysis of the problem, with a special emphasis on conservation and stability properties, and on the surface tension discretization are provided. Various numerical simulations are eventually presented. Some of them reproduce complex physical phenomena.

Key-words: magnetohydrodynamic; free interface; two-fluids flow, surface tension; geometric conservation law; ALE formulation.

* INRIA Rocquencourt - Projet M3N - e-mail: Jean-Frederic.Gerbeau@inria.fr
† CERMICS,Ecole Nationale des Ponts et Chaussées,6 & 8 Av. Pascal, 77455 Champs-sur-Marne, France, e-mail: lelievre@cermics.enpc.fr, lebris@cermics.enpc.fr

Unité de recherche INRIA Rocquencourt
Domaine de Voluceau, Rocquencourt, BP 105, 78153 Le Chesnay Cedex (France)
Téléphone : +33 1 39 63 55 11 —Télécopie : +33 1 39 63 53 30

Simulations d'écoulements MHD en présence d'interfaces mobiles

Résumé : Cette étude porte sur la simulation numérique d'un problème de magnétohydrodynamique à deux fluides qui se pose dans la production industrielle de l'aluminium. L'écoulement des deux fluides non miscibles est modélisé par les équations de Navier-Stokes couplées avec les équations de Maxwell. Le déplacement de l'interface séparant les deux fluides est pris en compte par une formulation Arbitraire Lagrange Euler. Des détails sur l'analyse numérique du problème, en particulier sur des questions de conservation et stabilité, ainsi que sur le calcul de la tension de surface sont présentés. Enfin, plusieurs simulations numériques sont proposées. Certaines d'entre elles reproduisent des phénomènes physiques complexes.

Mots-clés : magnétohydrodynamique, interface libre, écoulement à deux fluides, tension de surface, loi de conservation géométrique, formulation ALE

1 Introduction

The numerical simulation of the electrolysis cell for the industrial production of aluminium is a problem of outstanding difficulty. Let us briefly indicate that a schematic picture of the cell is as follows (*see* e.g. A.F. Lacamera *et al.* [22]) : an electric current of the order of 10^5 A runs through two horizontal layers of conducting incompressible fluids, namely a bath of an aluminium oxyde above, and a layer of liquid aluminium below (*see* Figure 1). With a view to reducing the energy cost, the distance between the carbon anode covering the top of the cell and the surface of the aluminium layer (a perfectly conducting fluid directly connected to the cathode at the bottom of the cell) is to be kept as small as possible. However, due to the presence of the electric current, the conducting fluids experience strong Lorentz forces and therefore move. This causes the interface separating the two fluids to also move, which may lead to instabilities. Ensuring a compromise between these two contradictory needs to have a small anode-aluminium distance in order to reduce the cost, and a large enough one in order to prevent short-circuits is the experimental challenge. Additional (substantial) difficulties (that will not be dealt with hereafter) come from the presence of a gas phase (carbon oxydes), from ferromagnetic effects on the boundary of the cell, and from solidification processes taking place on the edges of the cell.

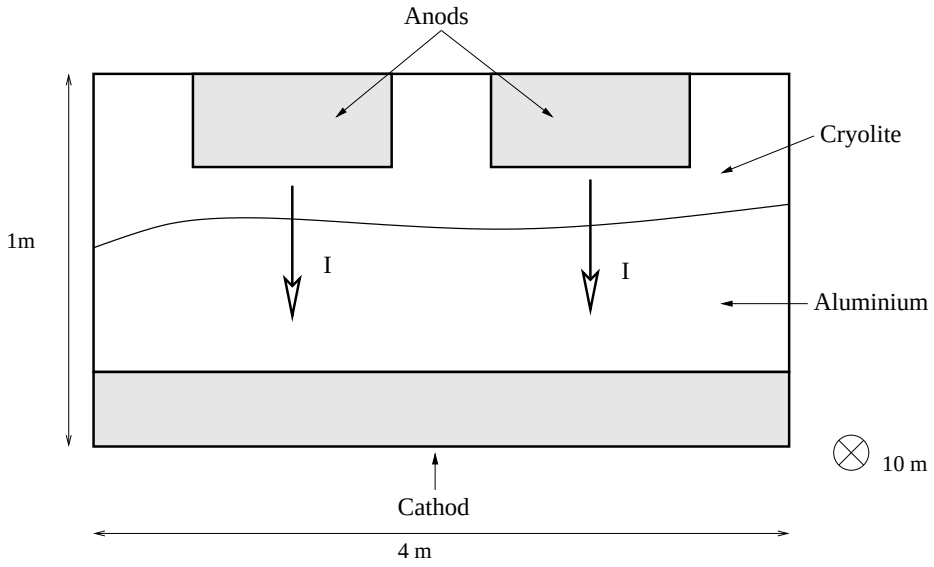

Figure 1: Schematic represention of an aluminium cell

The numerical simulation can efficiently complement the experiments in giving some insight into the working of the cell. There is indeed a large body of literature devoted to

such numerical simulations (*see* P.A. Davidson and R.I. Lindsay[3], J. Descloux *et al.* [4, 5] R. Moreau *et al.* [29, 30], M. Segatz and C. Droste [33], A.D. Sneyd and A. Wang [35]). Of course, in view of the large number of physical phenomena interacting with each other, a direct complete simulation of the cell cannot be achieved. At present, only partial simulations are available. Simplifying assumptions must be made. With a view to drawing a comparison with the numerous strategies based upon the linearization of the governing equations at the vicinity of a stationary solution (*see* e.g. [3]), we have decided to adopt a fully nonlinear strategy where no linearization is made.

The governing equations we shall discretize are the time-dependent incompressible Navier-Stokes equations for two viscous immiscible fluids coupled through Ohm's law with the Maxwell equations in their parabolic form (see equations (1)-(5) below). Let us emphasize that no additional simplification will be made on these equations and that we shall therefore deal with all the nonlinearities of this strongly coupled system of PDEs. The mathematical analysis of this system, as well as the foundation of it on the basis of a whole hierarchy of possible models, is an issue that has already been dealt with by two of us in a series of previous works (*see* [8, 10, 11, 12, 13]).

From the numerical viewpoint, the simulation of such a system requires to understand the following issues

- what type of finite elements should be used,
- how to ensure the conservation of the mass of each fluid and the energy stability in the time dependent simulation,
- how to deal with the motion of the interface, and to ensure, when necessary, the motion of the mesh,
- how to account properly for the surface tension effects when needed.

In the sequel, we shall detail how we have answered to these questions, but let us briefly say in this introduction that we use an Arbitray Lagrangian Eulerian formulation to move the interface and the mesh, that we take care of having a discrete energy inequality and a conservation of mass using a discretization scheme that ensures a geometric conservation law.

The article is organized as follows. Section 2 presents the governing equations in their dimensional and next adimensional form. In Section 3, we give details on the ALE formulation we use. Section 4 is devoted to the presentation of the global numerical algorithm. The conservation and stability properties of the discretization we have chosen are investigated in Section 5. A special attention is paid to the discretization of the surface tension term in Section 6. Finally, Section 7 presents numerical tests on academic as well as industrial situations.

Let us mention that an abridged version of this paper focusing on more practical aspects appears in [15].

2 The MHD equations for two fluids

2.1 Notations

As announced in the introduction, we consider a system consisting of two viscous incompressible non-miscible fluids in the presence of a magnetic field. The fluids fill in a fixed bounded domain Ω of $\mathbb{R}^d$ (with $d = 2$ or 3). The governing equations are the so-called incompressible MHD equations (*see* W.F. Hughes and F.J. Young [21] for example). We denote by ρ the density of the fluids, $\mathbf{u}$ the velocity field, $\mathbf{B}$ the magnetic field and p the pressure field. The electrical conductivity σ and the viscosity η are assumed to be known functions of ρ. Then, the following equations are satisfied in Ω:

$$\partial_t \rho + \operatorname{div}(\rho \mathbf{u}) = 0, \tag{1}$$

$$\rho \partial_t \mathbf{u} + \rho \mathbf{u} \cdot \nabla \mathbf{u} - \operatorname{div}(2\eta \boldsymbol{\epsilon}(\mathbf{u})) + \nabla p = \rho \mathbf{f} + \frac{1}{\mu} \mathbf{curl}\, \mathbf{B} \times \mathbf{B}, \tag{2}$$

$$\operatorname{div} \mathbf{u} = 0, \tag{3}$$

$$\partial_t \mathbf{B} + \mathbf{curl}\left(\frac{1}{\mu\sigma} \mathbf{curl}\, \mathbf{B}\right) = \mathbf{curl}\,(\mathbf{u} \times \mathbf{B}) \tag{4}$$

$$\operatorname{div} \mathbf{B} = 0, \tag{5}$$

where $\boldsymbol{\epsilon}(\mathbf{u}) = (\nabla \mathbf{u} + \nabla \mathbf{u}^T)/2$. For the sake of simplicity, we assume that

$$(\mathbf{B} \cdot \mathbf{n})|_{\partial\Omega} = 0, \tag{6}$$

$$(\mathbf{curl}\, \mathbf{B} \times \mathbf{n})|_{\partial\Omega} = 0. \tag{7}$$

As for the hydrodynamic boundary conditions, pure slip will be assumed on the side walls and no-slip elsewhere. We complement this system with the initial conditions:

$$\rho|_{t=0} = \rho^0, \quad \mathbf{u}|_{t=0} = \mathbf{u}^0 \quad \text{and} \quad \mathbf{B}|_{t=0} = \mathbf{B}^0, \tag{8}$$

where $\mathbf{u}^0$ and $\mathbf{B}^0$ are divergence free vector fields. The density of each fluid is assumed to be constant at $t = 0$: if x is in the domain occupied by the fluid i then $\rho^0(x) = \rho_i$, where ρ_i is a given constant, for $i = 1, 2$. Note that equation (1) implies that

$$\rho(x,t) = \rho_i \text{ for } x \text{ located in the fluid } i \text{ at time } t \quad (i = 1, 2). \tag{9}$$

We shall denote the jump of density through the interface by

$$\delta\rho = \rho_2 - \rho_1.$$

The viscosity and the electrical conductivity of each fluid are also assumed to be constant:

$$\eta(\rho_i) = \eta_i \quad \text{and} \quad \sigma(\rho_i) = \sigma_i \quad (i = 1, 2). \tag{10}$$

We refer the interested reader to [10] for an existence result of a weak solution to the system (1)-(5), and to [13] for the description of some numerical methods to impose the boundary conditions (6)-(7).

2.2 Non-dimensional form and body force correction

For computational purposes, it proves convenient to rewrite the preceeding equations in non-dimensional form and to eliminate the body force in one fluid, in the spirit of the method described in [14]. In practice, the body force $\mathbf{f}$ will be the gravity. Thus, it is sufficient to restrict oneself to the case when the body force is potential

$$\mathbf{f} = \nabla \Phi.$$

Characteristic values of the magnetic field B, of the velocity U and of the length L are introduced. Time and pressure characteristic values are then defined by $T = L/U$, $P = \rho_1 U^2$. The MHD system rewritten in terms of the non-dimensional variables x/L, t/T (still denoted by x and t) and $\tilde{\mathbf{u}} = \mathbf{u}/U$, $\tilde{\mathbf{B}} = \mathbf{B}/B$, and $\tilde{p} = p/P$, involves seven non-dimensional numbers:

$$\begin{aligned}
Re_i &= \frac{\rho_i U L}{\eta_i},\ i = 1,2, && \text{(Reynolds numbers)},\\
Rm_i &= \mu \sigma_i L U,\ i = 1,2, && \text{(magnetic Reynolds numbers)},\\
S &= \frac{B^2}{\mu \rho_1 U^2}, && \text{(coupling parameter)},\\
Fr &= \frac{U^2}{gL}, && \text{(Froude number)},\\
M &= \frac{\rho_2}{\rho_1}, && \text{(density ratio)}.
\end{aligned}$$

The non-dimensional potential of the body force is defined by $\tilde{\Phi} = \Phi/(gL)$ where g is the gravitational field strength. A "corrected pressure" $\tilde{P}$ is introduced:

$$\tilde{P} = \tilde{p} - \frac{M}{Fr}\tilde{\Phi}.$$

This allows to eliminate the body force in fluid 2. Although this trick does not change anything at the continuous level, it greatly improves the robustness of the numerical computations.

In fluid 1 (lower fluid, *i.e.* aluminium), the equations read

$$\begin{aligned}
\partial_t \tilde{\mathbf{u}} + \tilde{\mathbf{u}}.\nabla\tilde{\mathbf{u}} + \nabla\tilde{P} - \text{div}\left(\frac{2}{Re_1}\boldsymbol{\epsilon}(\tilde{\mathbf{u}})\right) &= \frac{1-M}{Fr}\nabla\tilde{\Phi} + S\,\mathbf{curl}\,\tilde{\mathbf{B}}\times\tilde{\mathbf{B}},\\
\partial_t \tilde{\mathbf{B}} + \mathbf{curl}\left(\frac{1}{Rm_1}\mathbf{curl}\,\tilde{\mathbf{B}}\right) &= \mathbf{curl}\,(\tilde{\mathbf{u}}\times\tilde{\mathbf{B}}),
\end{aligned}$$

and in fluid 2 (upper fluid, *i.e.* cryolite),

$$\begin{aligned}
M\partial_t \tilde{\mathbf{u}} + M\tilde{\mathbf{u}}.\nabla\tilde{\mathbf{u}} + \nabla\tilde{P} - \text{div}\left(\frac{M}{Re_2}\boldsymbol{\epsilon}(\tilde{\mathbf{u}})\right) &= S\,\mathbf{curl}\,\tilde{\mathbf{B}}\times\tilde{\mathbf{B}},\\
\partial_t \tilde{\mathbf{B}} + \mathbf{curl}\left(\frac{1}{Rm_2}\mathbf{curl}\,\tilde{\mathbf{B}}\right) &= \mathbf{curl}\,(\tilde{\mathbf{u}}\times\tilde{\mathbf{B}}).
\end{aligned}$$

3 Weak ALE formulation for two-fluid MHD flows

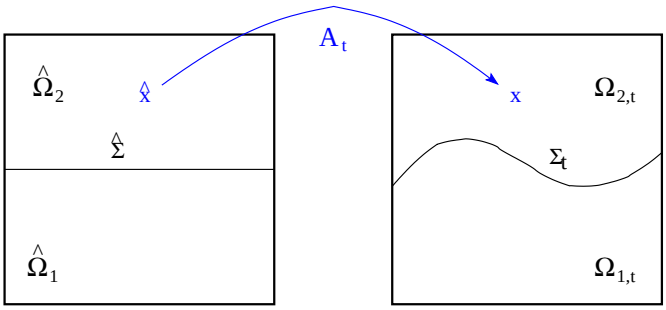

Figure 2: The partition of the domain Ω.

We tackle the problem of two fluids simulations with the so-called *Arbitrary Lagrangian Eulerian* (ALE) approach. Our computational grid therefore follows the physical interface. Although other methods have been investigated and have proven to be efficient in the past to simulate two-fluid flows, in particular on fixed grids (*see* for example R. Glowinski *et al.* [16]), the choice of the ALE approach is motivated here by two arguments: first, strong topological changes of the interface are not expected in our problem; second, a high precision on the position of the interface is of major interest in aluminium electrolysis simulations and we believe that such a precision can be obtained at a lower cost with ALE methods rather than with purely Eulerian ones. The ALE formulation for *one* fluid with a free surface has been used by several authors, *see* for example A. Soulaïmani *et al.* [36, 37], B. Maury [26], A. Huerta and W.K. Liu [20], R.A. Cairncross *et al.* [1, 2], L.W. Ho [19]. In the case of two fluids, *see* for example H.K. Rasmussen *et al.* [32].

We now introduce some notations. For $t > 0$, we denote the physical domain occupied by the fluid i by $\Omega_{i,t}$, for $i = 1, 2$. The domain Ω is the union of $\Omega_{1,t}$ and $\Omega_{2,t}$. The interface between $\Omega_{1,t}$ and $\Omega_{2,t}$ is denoted by Σ_t. The normal to Σ_t oriented from $\Omega_{1,t}$ to $\Omega_{2,t}$ is denoted by $\mathbf{n}$ and we set $\mathbf{n}_1 = \mathbf{n}$ and $\mathbf{n}_2 = -\mathbf{n}$. We define a reference configuration $\hat{\Omega} = \hat{\Omega}_1 \cup \hat{\Omega}_2$, $\hat{\Omega}_i$ being $\Omega_{i,t=0}$, and we consider a mapping $\hat{\mathcal{A}}_t$ which associates to a point $\hat{x} \in \hat{\Omega}$ a point $x \in \Omega$. Throughout, the mapping $\hat{\mathcal{A}}_t$ will be assumed to be smooth enough in $\hat{x}$, invertible with a smooth inverse, and differentiable with respect to t. For a function $\psi(\cdot, t)$ defined on Ω, we denote by $\hat{\psi}(\cdot, t)$ the function defined on $\hat{\Omega}$ satisfying $\hat{\psi}(\hat{x}, t) = \psi(x, t)$, with $x = \hat{\mathcal{A}}_t(\hat{x})$. By a classical abuse of notation, we will denote $\frac{\partial \psi}{\partial t}|_{\hat{x}}$ the time derivative on the ALE frame:

$$\frac{\partial \psi}{\partial t}\Big|_{\hat{x}}(x, t) = \frac{\partial \hat{\psi}}{\partial t}(\hat{x}, t), \qquad \text{with } \hat{x} = \hat{\mathcal{A}}_t^{-1}(x).$$

The domain velocity is defined by

$$\mathbf{w}(x,t) = \hat{\mathbf{w}}(\hat{x},t) = \frac{\partial \hat{\mathcal{A}}_t}{\partial t}(\hat{x}), \text{ with } \hat{x} = \hat{\mathcal{A}}_t^{-1}(x).$$

If $\boldsymbol{\nu}$ is the normal to $\partial\Omega$, the mapping $\hat{\mathcal{A}}_t$ is supposed to be such that

$$\mathbf{w} \cdot \boldsymbol{\nu} = 0 \qquad \text{on } \partial\Omega, \tag{11}$$

which means that the domain Ω is fixed in $\mathbb{R}^d$ and

$$\mathbf{u} \cdot \mathbf{n} = \mathbf{w} \cdot \mathbf{n} \qquad \text{on } \Sigma_t, \tag{12}$$

which means that the domains $\Omega_{1,t}$ and $\Omega_{2,t}$ follow the free interface. Thus,

$$\text{for } \hat{x} \in \hat{\Omega}_i, \quad x = \hat{\mathcal{A}}_t(\hat{x}) \in \Omega_{i,t}, \qquad i = 1,2. \tag{13}$$

Although the domains Ω and $\hat{\Omega}$ are in fact the same domain of $\mathbb{R}^d$, we will keep both notations for the sake of clarity.

We now recall some standard formulae which will be useful in the sequel. Otherwise explicitely mentioned, all the differential operators (∇, div, **curl**, ...) will be taken with respect to the eulerian variable x. We have

$$\left.\frac{\partial \psi}{\partial t}\right|_{\hat{x}}(x,t) = \frac{\partial \hat{\psi}}{\partial t}(\hat{x},t) = \frac{\partial \psi}{\partial t}(x,t) + \mathbf{w} \cdot \nabla\psi(x,t). \tag{14}$$

We denote by $\hat{\mathbf{J}}_t$ the Jacobian matrix of $\hat{\mathcal{A}}_t$,

$$\hat{\mathbf{J}}_t = \left[\frac{\partial \hat{\mathcal{A}}_t}{\partial \hat{x}_j}\right],$$

and by $\hat{J}_t$ its determinant. Then, we have the Euler formula,

$$\frac{\partial \hat{J}_t}{\partial t}(\hat{\mathcal{A}}_t^{-1}(x),t) = \hat{J}_t(\hat{\mathcal{A}}_t^{-1}(x),t)\,\mathrm{div}\,\mathbf{w}(x,t). \tag{15}$$

Using this relation we get in particular,

$$\begin{aligned}
\frac{d}{dt}\int_\Omega \psi(x,t)\,dx &= \frac{d}{dt}\int_{\hat{\Omega}} \hat{\psi}(\hat{x},t)\,\hat{J}_t\,d\hat{x} \\
&= \int_{\hat{\Omega}} \frac{\partial}{\partial t}(\hat{\psi}(\hat{x},t)\hat{J}_t)\,d\hat{x} \\
&= \int_{\hat{\Omega}} \left(\frac{\partial \hat{\psi}}{\partial t}(\hat{x},t)\,\hat{J}_t + \hat{\psi}(\hat{x},t)\hat{J}_t \mathrm{div}\,\mathbf{w}\right) d\hat{x}
\end{aligned}$$

and thus

$$\frac{d}{dt}\int_\Omega \psi(x,t)\,dx = \int_\Omega \frac{\partial \psi}{\partial t}\Big|_{\hat{x}}\,dx + \int_\Omega \psi(x,t)\,\mathrm{div}\,\mathbf{w}\,dx \tag{16}$$

We now propose a weak formulation of equations (1)-(5). The following functional spaces will be needed:

$$\mathbb{H}^1_0(\Omega) = \{\mathbf{v} \in (H^1(\Omega))^d, \mathbf{v} = 0 \text{ on } \partial\Omega\},$$
$$\mathbb{H}^1_n(\Omega) = \{\mathbf{C} \in (H^1(\Omega))^d, \mathbf{C}\cdot\mathbf{n} = 0 \text{ on } \partial\Omega\},$$

and $L^2_0(\Omega)$, the space of $L^2(\Omega)$ functions whose integral over Ω vanishes. We define

$$V = L^2(0,T;\mathbb{H}^1_0(\Omega)), \quad W = L^2(0,T;\mathbb{H}^1_n(\Omega)), \quad M = L^2(0,T;L^2_0(\Omega))$$

We will denote by $(\cdot,\cdot)$ the $(L^2(\Omega))^d$ scalar product

$$(\mathbf{u},\mathbf{v}) = \int_\Omega \mathbf{u}\cdot\mathbf{v}\,dx,$$

and we introduce the following bilinear and trilinear forms:

$$a_1(\mathbf{v}_1,\mathbf{v}_2) = \int_\Omega 2\eta\boldsymbol{\epsilon}(\mathbf{v}_1)\cdot\boldsymbol{\epsilon}(\mathbf{v}_2)\,dx,$$

$$a_2(\mathbf{C}_1,\mathbf{C}_2) = \int_\Omega \left(\frac{1}{\mu\sigma}\mathbf{curl}\,\mathbf{C}_1\cdot\mathbf{curl}\,\mathbf{C}_2 + \alpha\,\mathrm{div}\,\mathbf{C}_1\,\mathrm{div}\,\mathbf{C}_2\right)dx,$$

α being a given positive constant,

$$b(\mathbf{v},q) = \int_\Omega q\mathrm{div}\,\mathbf{v}\,dx,$$

$$c(\mathbf{v}_1,\mathbf{v}_2,\mathbf{v}_3) = \int_\Omega \mathbf{v}_1\cdot\nabla\mathbf{v}_2\cdot\mathbf{v}_3\,dx,$$

$$c_{\mathbf{w}}(\mathbf{v}_1,\mathbf{v}_2,\mathbf{v}_3) = \int_\Omega \rho\,(\mathbf{v}_1-\mathbf{w})\cdot\nabla\mathbf{v}_2\cdot\mathbf{v}_3\,dx,$$

$$d(\mathbf{v}_1,\mathbf{v}_2,\mathbf{v}_3) = \int_\Omega \mathbf{v}_2\cdot\mathbf{v}_3\,\mathrm{div}\,\mathbf{v}_1\,dx,$$

$$l(\mathbf{v},\mathbf{C}_1,\mathbf{C}_2) = \int_\Omega \mathbf{v}\times\mathbf{C}_1\cdot\mathbf{curl}\,\mathbf{C}_2\,dx.$$

We introduce the test function spaces on the reference domain

$$\hat{V} = \mathbb{H}^1_0(\hat{\Omega}), \qquad \hat{W} = \mathbb{H}^1_n(\hat{\Omega}), \qquad \hat{M} = L^2_0(\hat{\Omega}).$$

On the current domain, the test function spaces are defined by

$$V_0 = \{\mathbf{v} : \Omega \times [0,T] \to \mathbb{R}^d,\ \mathbf{v}(x,t) = \hat{\mathbf{v}}(\hat{\mathcal{A}}_t^{-1}(x)), \hat{\mathbf{v}} \in \hat{V}\},$$

$$W_0 = \{\mathbf{C} : \Omega \times [0,T] \to \mathbb{R}^d,\ \mathbf{C}(x,t) = \hat{\mathbf{C}}(\hat{\mathcal{A}}_t^{-1}(x)), \hat{\mathbf{C}} \in \hat{W}\},$$

$$M_0 = \{q : \Omega \times [0,T] \to \mathbb{R},\ q(x,t) = \hat{q}(\hat{\mathcal{A}}_t^{-1}(x)), \hat{q} \in \hat{M}\}.$$

It is worth noticing that the test functions do not depend on t on the reference frame whereas they do on the current one. More precisely, denoting by $(v_i)_{i=1,..,d}$ the components of $\mathbf{v} \in V_0$, we have

$$\left.\frac{\partial v_i}{\partial t}\right|_{\hat{x}} = \frac{\partial v_i}{\partial t} + \mathbf{w} \cdot \nabla v_i = 0. \tag{17}$$

Of course, similar relations hold for the functions of W_0 and M_0. We now give the formulation that will be used in the numerical simulations.

Weak ALE formulation: Suppose that the domain is moving as described above (in particular relations (11) and (12) are satisfied). We compute the density ρ simply by

$$\rho(x,t) = \rho^0(\hat{x}) = \rho_i \qquad \text{for } x \in \Omega_{i,t} \tag{18}$$

and we look for $(\mathbf{u}, \mathbf{B}, p)$ in $V \times W \times M$ such that, for all $(\mathbf{v}, \mathbf{C}, q)$ in $V_0 \times W_0 \times M_0$:

$$\begin{aligned} \frac{d}{dt}(\rho\mathbf{u}, \mathbf{v}) + a_1(\mathbf{u}, \mathbf{v}) + c_{\mathbf{w}}(\mathbf{u}, \mathbf{u}, \mathbf{v}) - d(\mathbf{w}, \rho\mathbf{u}, \mathbf{v}) & \\ + b(\mathbf{v}, p) + \frac{1}{\mu} l(\mathbf{v}, \mathbf{B}, \mathbf{B}) &= (\rho\mathbf{f}, \mathbf{v}), \qquad (19) \\ b(\mathbf{u}, q) &= 0, \qquad (20) \\ \frac{d}{dt}(\mathbf{B}, \mathbf{C}) + a_2(\mathbf{B}, \mathbf{C}) - c(\mathbf{w}, \mathbf{B}, \mathbf{C}) - d(\mathbf{w}, \mathbf{B}, \mathbf{C}) &= l(\mathbf{u}, \mathbf{B}, \mathbf{C}). \qquad (21) \end{aligned}$$

Proposition 1
System (1)-(5) is formally equivalent to the weak ALE formulation (18)-(21).

Proof. Let $(\rho, \mathbf{u}, \mathbf{B}, p)$ be a solution to (1)-(5). Equation (1) clearly yields (18). As for the momentum equation (19), using formula (14), we have from (2)

$$\rho \partial_t \mathbf{u}|_{\hat{x}} + \rho(\mathbf{u} - \mathbf{w}) \cdot \nabla \mathbf{u} = \mathbf{g},$$

with $\mathbf{g} = \rho\mathbf{f} - \nabla p + \operatorname{div}(2\eta\boldsymbol{\epsilon}(\mathbf{u})) + \frac{1}{\mu}\mathbf{curl}\,\mathbf{B} \times \mathbf{B}$. We multiply this equation by $\mathbf{v} \in V_0$ and we integrate on Ω:

$$\int_\Omega \rho \left.\frac{\partial \mathbf{u}}{\partial t}\right|_{\hat{x}} \cdot \mathbf{v}\, dx + \int_\Omega \rho(\mathbf{u} - \mathbf{w}) \cdot \nabla \mathbf{u} \cdot \mathbf{v}\, dx = \int_\Omega \mathbf{g} \cdot \mathbf{v}\, dx.$$

Using (16), (17) and (18), we can write the first term as follows

$$\int_\Omega \rho \frac{\partial \mathbf{u}}{\partial t}\Big|_{\hat{x}} \cdot \mathbf{v}\, dx = \int_\Omega \frac{\partial}{\partial t}\Big|_{\hat{x}} (\rho\, \mathbf{u}\cdot\mathbf{v})\, dx = \frac{d}{dt}\int_\Omega \rho\, \mathbf{u}\cdot\mathbf{v}\, dx - \int_\Omega \rho \mathbf{u}\cdot\mathbf{v}\mathrm{div}\, \mathbf{w}\, dx.$$

Thus the momentum equation reads

$$\frac{d}{dt}\int_\Omega \rho\mathbf{u}\cdot\mathbf{v}\, dx + \int_\Omega \rho(\mathbf{u}-\mathbf{w})\cdot\nabla\mathbf{u}\cdot\mathbf{v}\, dx - \int_\Omega \rho\mathbf{u}\cdot\mathbf{v}\mathrm{div}\, \mathbf{w}\, dx = \int_\Omega \mathbf{g}\cdot\mathbf{v}\, dx.$$

Then, classical integration by parts on the right-hand side of this equation gives (19).

Analogous computations give the left-hand side of equation (21) and its right-hand side is a straightforward consequence of the formula

$$\int_\Omega \mathbf{curl}\,\mathbf{B}\cdot\mathbf{C}\, dx = \int_\Omega \mathbf{B}\cdot\mathbf{curl}\,\mathbf{C}\, dx + \int_{\partial\Omega} \mathbf{n}\times\mathbf{B}\cdot\mathbf{C}\, dx.$$

and the boundary condition (7).

Conversely, suppose that $(\rho, \mathbf{u}, \mathbf{B}, p)$ is a solution to the weak ALE formulation (18)-(21). With (18), it is clear that

$$\frac{\partial \rho}{\partial t}\Big|_{\hat{x}} = 0. \tag{22}$$

Moreover, using (12),

$$(\mathbf{u}-\mathbf{w})\cdot\nabla\rho = \delta\rho\, \mathbf{n}\cdot(\mathbf{u}-\mathbf{w})|_{\Sigma_t} = 0.$$

Therefore, with (14),

$$\partial_t\rho + \mathrm{div}\,(\rho\mathbf{u}) = \partial_t\rho + \mathbf{u}\cdot\nabla\rho = \partial_t\rho|_{\hat{x}} + (\mathbf{u}-\mathbf{w})\cdot\nabla\rho = 0,$$

which proves (at least formally) that (1) holds. The same manipulations as above show that (2) and (4) hold, and the continuity relation (3) is a clear consequence of (20).

We now turn to relation (5). Let $\hat{\phi} \in H^2(\hat{\Omega})$, with $\frac{\partial\phi}{\partial\mathbf{n}} = 0$ on $\partial\Omega$. Taking $\nabla\phi$ as a test function in (21), using (14) and (16) , we obtain

$$\int_\Omega \partial_t\mathbf{B}\cdot\nabla\phi\, dx + \alpha\int_\Omega \mathrm{div}\,(\nabla\phi)\,\mathrm{div}\,\mathbf{B} = 0.$$

Using $\frac{\partial\phi}{\partial\mathbf{n}} = 0$ and $\mathbf{B}\cdot\mathbf{n} = 0$ on $\partial\Omega$, this gives

$$\int_\Omega (\partial_t \mathrm{div}\,\mathbf{B} - \alpha\triangle(\mathrm{div}\,\mathbf{B}))\phi\, dx = -\alpha\int_{\partial\Omega} \frac{\partial(\mathrm{div}\,\mathbf{B})}{\partial\mathbf{n}}\phi\, d\sigma.$$

Thus

$$\begin{cases} \partial_t \mathrm{div}\,\mathbf{B} - \alpha\triangle(\mathrm{div}\,\mathbf{B}) &= 0 \quad \text{in } \Omega, \\ \dfrac{\partial(\mathrm{div}\,\mathbf{B})}{\partial\mathbf{n}} &= 0 \quad \text{on } \partial\Omega, \end{cases}$$

Using $\mathrm{div}\,\mathbf{B}^0 = 0$, this implies (5). ♢

4 Discretization

The goal of this section is to present the space and time discretizations that are used to solve the system (19)-(21). For this purpose, we introduce a new trilinear form $\tilde{c}_{\mathbf{w}}$ which is a slight modification of $c_{\mathbf{w}}$:

$$\begin{aligned}\tilde{c}_{\mathbf{w}}(\mathbf{v}_1,\mathbf{v}_2,\mathbf{v}_3) = c_{\mathbf{w}}(\mathbf{v}_1,\mathbf{v}_2,\mathbf{v}_3) + \frac{1}{2}\int_\Omega \rho \,\mathrm{div}\,\mathbf{v}_1\,\mathbf{v}_2\cdot\mathbf{v}_3\,dx \\ + \frac{\delta\rho}{2}\int_{\Sigma_t}(\mathbf{v}_1-\mathbf{w})\cdot\mathbf{n}\,\mathbf{v}_2\cdot\mathbf{v}_3\,d\sigma\end{aligned} \tag{23}$$

Note that at the continuous level, relations (3) and (12) yield

$$c_{\mathbf{w}}(\mathbf{u},\mathbf{u},\mathbf{v}) = \tilde{c}_{\mathbf{w}}(\mathbf{u},\mathbf{u},\mathbf{v}).$$

The first integral in (23) is analogous to the well-known Temam's term that allows to recover at the discrete level, when the density is constant, the skew-symmetry property of the advection term. The second integral is less standard. Its introduction will be motivated in Section 5.3 (see equation (34)). Note that the normal vectors $\mathbf{n}$ introduced here are not the approximated node normals defined below (Section 5.2, formula (28)) but rather the "real" normals defined almost everywhere on the interface, and in particular on the Gauss-Legendre integration points located inside the elements.

4.1 Space discretization

We consider a finite element discretization of the current domain Ω. The finite element spaces for the velocity, the magnetic field and the pressure are respectively denoted by

$$V_h \subset (H_0^1(\Omega))^d, \qquad W_h \subset (H_n^1(\Omega))^d, \qquad M_h \subset L_0^2(\Omega).$$

In our numerical tests, V_h and W_h are always based on the same same Lagrangian finite element. We use either stable or stabilized spaces. By "stable spaces", we mean a pair (V_h, M_h) of spaces satisfying the following standard inf-sup condition

$$\inf_{p\in M_h}\sup_{\mathbf{v}_h\in V_h}\frac{b(\mathbf{v}_h,q)}{\|\mathbf{v}_h\|_{\mathbb{H}^1}\,\|q\|_{L^2}} \geq \beta > 0.$$

We refer the reader to M.D. Gunzburger *et al.* [18] for a complete analysis of the stable spaces for the stationary MHD equations. In the computations with stable elements, we used Q2 elements for the velocity and the magnetic field and, either discontinuous piecewise P1 or continuous piecewise Q1 elements for the pressure. On the other hand, the stabilized finite elements spaces that we use are based on the formulation proposed in [9]. This choice allows us to use equal order finite elements for the three unknown fields (typically Lagrangian Q1 finite elements) and improves the stability at high Reynolds numbers.

4.2 Time discretization and linearization

We denote by Ω_i^n the domain occupied by the fluid i at time t_n and by $\mathbf{w}_n$ the approximated domain velocity at time t_n. We introduce the application $\mathcal{A}_{n,n+1} : \Omega \longrightarrow \Omega$, such that $\mathcal{A}_{n,n+1}$ maps Ω_i^n onto Ω_i^{n+1}, for $i = 1, 2$:

$$x = \mathcal{A}_{n,n+1}(y) = y + \delta t \mathbf{w}^n(y), \qquad \text{for } y \in \Omega_i^n.$$

Whenever it improves the clarity, y will denote the points in Ω_i^n and x the points in Ω_i^{n+1}. We denote by $\mathbf{J}_{n,n+1}$ the Jacobian matrix of $\mathcal{A}_{n,n+1}$,

$$\mathbf{J}_{n,n+1} = \left[\frac{\partial \mathcal{A}_{n,n+1}}{\partial y_j}\right],$$

and by $J_{n,n+1}$ the absolute value of its determinant.

We use the following semi-implicit Euler scheme:

$$\left\{\begin{array}{rl} \dfrac{1}{\delta t}(\rho\mathbf{u}^{n+1},\mathbf{v})^{n+1} + a_1^{n+1}(\mathbf{u}^{n+1},\mathbf{v}) + \tilde{c}_{\mathbf{w}^n}^{n+1}(\mathbf{u}^n,\mathbf{u}^{n+1},\mathbf{v}) & \\ -d^{n+1}(\mathbf{w}^n,\rho\mathbf{u}^{n+1},\mathbf{v}) + b^{n+1}(\mathbf{v},p^{n+1}) + \dfrac{1}{\mu}l^{n+1}(\mathbf{v},\mathbf{B}^n,\mathbf{B}^{n+1}) = & (\rho\mathbf{f}^{n+1},\mathbf{v})^{n+1} \\ & +\dfrac{1}{\delta t}(\rho\mathbf{u}^n,\mathbf{v})^n, \\ b^{n+1}(\mathbf{u}^{n+1},q) = & 0, \\ \dfrac{1}{\delta t}(\mathbf{B}^{n+1},\mathbf{C})^{n+1} + a_2^{n+1}(\mathbf{B}^{n+1},\mathbf{C}) - c^{n+1}(\mathbf{w}^n,\mathbf{B}^{n+1},\mathbf{C}) & \\ -d^{n+1}(\mathbf{w}^n,\mathbf{B}^{n+1},\mathbf{C}) - l^{n+1}(\mathbf{u}^{n+1},\mathbf{B}^n,\mathbf{C}) = & \dfrac{1}{\delta t}(\mathbf{B}^n,\mathbf{C})^n. \end{array}\right. \tag{24}$$

The superscripts on the forms $(\cdot,\cdot)$, a_1, a_2, b, c, d and l indicate the configuration on which the space integrals are performed. For example:

$$(\rho\mathbf{u}^{n+1},\mathbf{v})^{n+1} = \int_{\Omega^{n+1}} \rho\mathbf{u}^{n+1}\cdot\mathbf{v}\,dx = \sum_{i=1,2}\rho_i\int_{\Omega_i^{n+1}}\mathbf{u}^{n+1}\cdot\mathbf{v}\,dx,$$

$$(\rho\mathbf{u}^n,\mathbf{v})^n = \int_{\Omega^n}\rho\mathbf{u}^n\cdot\mathbf{v}\,dx = \sum_{i=1,2}\rho_i\int_{\Omega_i^n}\mathbf{u}^n\cdot\mathbf{v}\,dy,$$

$$a_1^{n+1}(\mathbf{u}^{n+1},\mathbf{v}) = \int_{\Omega^{n+1}} 2\,\eta\,\boldsymbol{\epsilon}(\mathbf{u}^{n+1})\cdot\boldsymbol{\epsilon}(\mathbf{v})\,dx = \sum_{i=1,2} 2\,\eta_i\int_{\Omega_i^{n+1}}\boldsymbol{\epsilon}(\mathbf{u}^{n+1})\cdot\boldsymbol{\epsilon}(\mathbf{v})\,dx,$$

$$\begin{aligned}\tilde{c}_{\mathbf{w}^n}^{n+1}(\mathbf{u}^n,\mathbf{u}^{n+1},\mathbf{v}) = &\sum_{i=1,2}\rho_i\int_{\Omega_i^{n+1}}\left[(\mathbf{u}^n-\mathbf{w}^n)\cdot\nabla\mathbf{u}^{n+1}\cdot\mathbf{v} + \frac{1}{2}\mathrm{div}\,\mathbf{u}^n\mathbf{u}^{n+1}\cdot\mathbf{v}\right]dx \\ &+\frac{\delta\rho}{2}\int_{\Sigma^{n+1}}(\mathbf{u}^n-\mathbf{w}^n)\cdot\mathbf{n}\,\mathbf{u}^{n+1}\cdot\mathbf{v}\,d\sigma.\end{aligned}$$

Note that in the latter formula, $\mathbf{u}^n$ is a shortcut for $\mathbf{u}^n \circ \mathcal{A}_{n,n+1}^{-1}(x)$. The other definitions for l, b, d, a_2 can be deduced straightforwardly.

We emphasize that the system to be solved at each time step is now linear but that the hydrodynamic and magnetic equations are still coupled through the terms $l^{n+1}(\mathbf{v}, \mathbf{B}^n, \mathbf{B}^{n+1})$ and $l^{n+1}(\mathbf{u}^{n+1}, \mathbf{B}^n, \mathbf{C})$. As will be shown in Section 5.3, this choice is one of the ingredients of the stability property of the scheme.

4.3 Global algorithm

In order to describe the global algorithm, we still have to define precisely the mesh motion. The basic requirements are to satisfy the kinematic conditions (11) and (12). Next, we have to choose how to move the points inside the domain. Many solutions have been proposed in the literature. For example, we refer to R.A. Cairncross *et al.* [2] for a presentation of a method adapted to the cases when the mesh experiences large strains. In the practical problem we are interested in, it seems sufficient to adopt the very standard method that consists in solving a simple Poisson problem to compute the velocity of the mesh. Moreover, we choose to constrain the displacement to be purely vertical. This choice, which is definitely reasonable in the physical situation that we consider, has important consequences on the quality of the algorithm. This point will be made precise in the next section.

We may now write the global algorithm. Let us be given Ω^n and $(\mathbf{u}^n, \mathbf{B}^n, p^n)$, Ω^{n+1} and $(\mathbf{u}^{n+1}, \mathbf{B}^{n+1}, p^{n+1})$ are computed as follows:

(i) Compute the terms on Ω_n (namely $\frac{1}{\delta t}\int_{\Omega^n} \rho^n \mathbf{u}^n \cdot \mathbf{v}\, dx$ and $\frac{1}{\delta t}\int_{\Omega^n} \mathbf{B}^n \cdot \mathbf{C}\, dx$)).

(ii) Compute $\mathbf{w}^n = (0, 0, w)$ with w such that

$$\begin{cases} -\triangle w = 0, & \text{on } \Omega_i^n, i = 1, 2 \\ w = \mathbf{u}^n \cdot \mathbf{n}/n_z, & \text{on } \Sigma^n, \\ \dfrac{\partial w}{\partial n} = 0 & \text{on } \partial\Omega, \end{cases} \tag{25}$$

(iii) Move the mesh: $\Omega^{n+1} = \Omega^n + \delta t\, \mathbf{w}^n$. The matrix corresponding to system (24) is computed on this new domain.

(iv) Solve (24) to determine $(\mathbf{u}^{n+1}, \mathbf{B}^{n+1}, p^{n+1})$. The resolution is performed by a GMRES iterative procedure with an ILU preconditioner and $(\mathbf{u}^n, \mathbf{B}^n, p^n)$ as the initial guess.

5 Conservation and stability properties

In this section, two important properties of the above algorithm are proved: the mass conservation, and the energy stability.

5.1 Geometric conservation law

Lemma 1

Suppose that the domain velocity $\mathbf{w}^n$ *has the form* $(0,0,w)$*. Let* ψ *be a function defined on* Ω_i^{n+1}*, for* $i = 1$ *or 2. Then*

$$\int_{\Omega_i^{n+1}} \psi(x)\,dx - \int_{\Omega_i^n} \psi \circ \mathcal{A}_{n,n+1}(y)\,dy = \delta t \int_{\Omega_i^n} \psi \circ \mathcal{A}_{n,n+1}(y) \mathrm{div}_y \mathbf{w}^n\,dy \tag{26}$$

$$= \delta t \int_{\Omega_i^{n+1}} \psi(x) \mathrm{div}_x \mathbf{w}^n \circ \mathcal{A}_{n,n+1}^{-1}(x)\,dx. \tag{27}$$

Proof. The change of variable defined by $x = \mathcal{A}_{n,n+1}(y)$ gives in the first integral:

$$\int_{\Omega_i^{n+1}} \psi(x)\,dx = \int_{\Omega_i^n} \psi \circ \mathcal{A}_{n,n+1}(y) J_{n,n+1}\,dy.$$

With the assumption on the mesh velocity, the Jacobian matrix has the following form

$$\mathbf{J}_{n,n+1} = \begin{bmatrix} 1 & 0 & 0 \\ 0 & 1 & 0 \\ \delta t \frac{\partial w}{\partial y_1} & \delta t \frac{\partial w}{\partial y_2} & 1 + \delta t \frac{\partial w}{\partial y_3} \end{bmatrix},$$

and therefore

$$J_{n,n+1} = 1 + \delta t \mathrm{div}_y \mathbf{w}^n,$$

which concludes the proof of the first relation (26).

For relation (27), we perform in the second integral of the left-hand side the change of variable defined by $y = \mathcal{A}_{n,n+1}^{-1}(x)$. Noticing that $y = x - \delta t \mathbf{w}^n \circ \mathcal{A}_{n,n+1}^{-1}(x)$, analogous computations as with the proof of (26) give:

$$\int_{\Omega_i^n} \psi(\mathcal{A}_{n,n+1}(y))\,dy = \int_{\Omega_i^{n+1}} \psi(x)(1 - \delta t \mathrm{div}_x \mathbf{w}^n \circ \mathcal{A}_{n,n+1}^{-1}(x))\,dx,$$

which is (27). ◊

Relations (26) and (27) can be viewed as discrete counterparts of relation (16). There are related to the so-called *geometric conservation law* (hereafter abbreviated as GCL).

The notion of GCL has been much investigated in the framework of the finite volume method, *see* in particular H. Guillard and C. Farhat [17], M. Lesoinne and C. Farhat [25], B. Nkonga and H. Guillard [31]. H. Guillard and C. Farhat prove in [17] that the GCL is a sufficient condition for a numerical scheme to be first-order time-accurate on a moving grid, independently of the grid motion. More generally, these authors claim that a higher accuracy is obtained with schemes satisfying the GCL compared to the schemes that violate it and that the schemes satisfying the GCL generally allow for a larger time step. In the framework of finite element methods, F. Nobile and L. Formaggia prove in [7] that the GCL is a sufficient condition to ensure the unconditional stability of a backward Euler scheme

applied to an advection diffusion equation on a moving domain. Let us also cite the work by P. Le Tallec and J. Mouro [24] where implications of the GCL in the framework of fluid structure interaction problems are discussed.

In the sequel, we will show that (26) and (27) are key properties to ensure discrete mass conservation and global energy inequality.

5.2 Discrete mass conservation

We now present the ingredients that allows us to obtain an exact mass conservation of each fluid after time and space discretization.

The first ingredient is the computation of the normals. It is convenient, in view of enforcing Dirichlet boundary conditions in (25), to compute approximated discrete normals at the *nodes* of the interface. But these approximation must be done carefully. More precisely, let i be a node on the interface Σ^n and let φ_i be the basis function associated to this node. We define $\mathbf{n}_{1,i}$ by

$$\mathbf{n}_{1,i} = \frac{1}{\int_{\Sigma^n} \varphi_i \, d\sigma} \int_{\Omega_1^n} \nabla \varphi_i \, dx \tag{28}$$

Note that, if we define $\mathbf{n}_{2,i}$ by substituting Ω_1^n by Ω_2^n in (28), it is straightforward to check that $\mathbf{n}_{1,i} = -\mathbf{n}_{2,i}$. We then define $\mathbf{n}_i = \mathbf{n}_{1,i}$ the approximated normal, on node i, oriented from Ω_1^n to Ω_2^n. The component of $\mathbf{n}_i$ are denoted by $(n_i^{(1)}, n_i^{(2)}, n_i^{(3)})$. Let $\mathbf{v}_h$ be an element of V_h whose components are $(v^{(1)}, v^{(2)}, v^{(3)})$. By convention, we denote

$$\mathbf{v}_h \cdot \mathbf{n}_h = \sum_i (v_i^{(1)} n_i^{(1)} + v_i^{(2)} n_i^{(2)} + v_i^{(3)} n_i^{(3)}) \varphi_i.$$

Then, formula (28) yields the following key property: let $\mathbf{v}_h^1$ (resp. $\mathbf{v}_h^2$) be a function of V_h whose support is included in Ω_1^n (resp. Ω_2^n), then

$$\int_{\Omega_1^n} \operatorname{div} \mathbf{v}_h^1 \, dx = \int_{\Sigma^n} \mathbf{v}_h^1 \cdot \mathbf{n}_h \, d\sigma, \quad \text{and} \quad \int_{\Omega_2^n} \operatorname{div} \mathbf{v}_h^2 \, dx = -\int_{\Sigma^n} \mathbf{v}_h^2 \cdot \mathbf{n}_h \, d\sigma. \tag{29}$$

The second ingredient to ensure mass conservation is to satisfy the following property:

$$\int_{\Omega_i^n} \operatorname{div} \mathbf{u}_h^n \, dx = 0, \qquad \text{for } i = 1, 2. \tag{30}$$

This can be achieved either by using a space of *discontinuous* finite elements for the discretization of the pressure (for example with the mixed elements Q2/P1), or by imposing with a Lagrange multiplier that the numerical flux through the interface vanishes:

$$\int_{\Sigma^n} \mathbf{u}_h^n \cdot \mathbf{n}_h \, d\sigma = 0. \tag{31}$$

For more details on this latter strategy, we refer the interested reader to L. Formaggia *et al.* [6]. We have tested the two approaches, and they both give the expected results. Another interesting possibility that we have however not investigated is to use continuous finite element for the pressure on each fluid, but discontinuous on the interface.

On a fixed domain, the two relations (29) and (30) would be sufficient to ensure the mass conservation. But the GCL property of Lemma 1 will be needed to extend it to the case of moving domains.

Proposition 2
If the discrete normals to the interface and the discrete velocity are computed in such a way that formula (29) and (30) are true, and if the motion of the mesh is such that (26) is satisfied, then the mass of each fluid is preserved:

$$\rho_i|\Omega_i^n| = \rho_i|\Omega_i^{n+1}|, \text{ for } i = 1, 2,$$

where $|\Omega_i^n|$ *denotes the measure of* Ω_i^n.

Proof. Relation (26) gives with $\psi = \rho_i$

$$\rho_i|\Omega_i^{n+1}| - \rho_i|\Omega_i^n| = \delta t \rho_i \int_{\Omega_i^n} \mathrm{div}_y \mathbf{w}_h^n \, dy.$$

Thus, using successively (29), (12) and (30), we have

$$\begin{aligned}\rho_i|\Omega_i^{n+1}| - \rho_i|\Omega_i^n| &= \delta t \rho_i \int_{\Sigma^n} \mathbf{w}_h^n \cdot \mathbf{n}_i \, d\sigma \\ &= \delta t \rho_i \int_{\Sigma^n} \mathbf{u}_h^n \cdot \mathbf{n}_i \, d\sigma \\ &= \delta t \rho_i \int_{\Omega_i^n} \mathrm{div}_y \mathbf{u}_h^n \, dy = 0.\end{aligned}$$

◊

5.3 Discrete energy inequality

It is assumed throughout this section that stable finite element spaces are used.

Proposition 3
We denote by

$$E^n = \int_{\Omega^n} \frac{\rho|\mathbf{u}^n|^2}{2} \, dy + \int_{\Omega^n} \frac{|\mathbf{B}^n|^2}{2\mu} \, dy \tag{32}$$

the total energy of the system at time t^n. *If the body force* $\mathbf{f}$ *vanishes, the solution computed by the algorithm of Section 4.3 satisfies the energy inequality*

$$\frac{E^{n+1} - E^n}{\delta t} + \int_{\Omega^{n+1}} 2\eta|\epsilon(\mathbf{u}^{n+1})|^2 \, dx + \int_{\Omega^{n+1}} \frac{1}{\mu\sigma}|\mathbf{curl}\,\mathbf{B}^{n+1}|^2 \, dx \leq 0.$$

Proof. We take $\mathbf{v} = \mathbf{u}^{n+1}$ in the hydrodynamic equation and $C = \frac{1}{\mu}\mathbf{B}^{n+1}$ in the magnetic equation.

The first argument of the proof is once again based on the GCL. Elementary manipulations give

$$\frac{1}{\delta t}\int_{\Omega^{n+1}} \rho|\mathbf{u}^{n+1}|^2\,dx - \frac{1}{\delta t}\int_{\Omega^n} \rho\mathbf{u}^n\cdot\mathbf{u}^{n+1}\,dy = \frac{1}{\delta t}\int_{\Omega^{n+1}} \rho|\mathbf{u}^{n+1}|^2\,dx$$
$$-\frac{1}{2\delta t}\int_{\Omega^n} \rho|\mathbf{u}^{n+1}|^2\,dy - \frac{1}{2\delta t}\int_{\Omega^n} \rho|\mathbf{u}^n|^2\,dy + \frac{1}{2\delta t}\int_{\Omega^n} \rho|\mathbf{u}^{n+1}-\mathbf{u}^n|^2\,dy.$$

Then, using Lemma 1, we obtain

$$\frac{1}{\delta t}\int_{\Omega^{n+1}} \rho|\mathbf{u}^{n+1}|^2\,dx - \frac{1}{\delta t}\int_{\Omega^n} \rho|\mathbf{u}^{n+1}|^2\,dy = \int_{\Omega^{n+1}} \rho|\mathbf{u}^{n+1}|^2\mathrm{div}\,\mathbf{w}^n\,dx,$$

and therefore

$$\begin{aligned}\frac{1}{\delta t}\int_{\Omega^{n+1}} \rho|\mathbf{u}^{n+1}|^2\,dx - \frac{1}{\delta t}\int_{\Omega^n} \rho\mathbf{u}^{n+1}\cdot\mathbf{u}^n\,dy = \\ \frac{1}{2\delta t}\int_{\Omega^{n+1}} \rho|\mathbf{u}^{n+1}|^2\,dx - \frac{1}{2\delta t}\int_{\Omega^n} \rho|\mathbf{u}^n|^2\,dy \\ +\frac{1}{2\delta t}\int_{\Omega^n} \rho|\mathbf{u}^{n+1}-\mathbf{u}^n|^2\,dy + \frac{1}{2}\int_{\Omega^{n+1}} \rho|\mathbf{u}^{n+1}|^2\mathrm{div}\,\mathbf{w}^n\,dx.\end{aligned} \tag{33}$$

Following the same idea, a similar relation can be straightforwardly obtained for the magnetic field.

The second argument is to use the "correction" that we have performed on the advection term. Definition (23) gives

$$\tilde{c}^{n+1}_{\mathbf{w}^n}(\mathbf{u}^n,\mathbf{u}^{n+1},\mathbf{u}^{n+1}) = \int_{\Omega^{n+1}} \rho(\mathbf{u}^n-\mathbf{w}^n)\cdot\nabla\left(\frac{|\mathbf{u}^{n+1}|^2}{2}\right)dx$$
$$+\frac{1}{2}\int_{\Omega^{n+1}} \rho|\mathbf{u}^{n+1}|^2\mathrm{div}\,\mathbf{u}^n\,dx + \frac{\delta\rho}{2}\int_{\Sigma^{n+1}} (\mathbf{u}^n-\mathbf{w}^n)\cdot\mathbf{n}|\mathbf{u}^{n+1}|^2\,d\sigma$$

The first integral reads

$$\int_{\Omega^{n+1}} \rho(\mathbf{u}^n-\mathbf{w}^n)\cdot\nabla\left(\frac{|\mathbf{u}^{n+1}|^2}{2}\right)dx = -\frac{1}{2}\int_{\Omega^{n+1}} |\mathbf{u}^{n+1}|^2\mathrm{div}\,(\rho(\mathbf{u}^n-\mathbf{w}^n))\,dx$$
$$= -\frac{1}{2}\int_{\Omega^{n+1}} \rho|\mathbf{u}^{n+1}|^2\mathrm{div}\,(\mathbf{u}^n-\mathbf{w}^n)\,dx - \frac{\delta\rho}{2}\int_{\Sigma^{n+1}} (\mathbf{u}^n-\mathbf{w}^n)\cdot\mathbf{n}|\mathbf{u}^{n+1}|^2\,d\sigma.$$

Thus,

$$\tilde{c}^{n+1}_{\mathbf{w}^n}(\mathbf{u}^n,\mathbf{u}^{n+1},\mathbf{u}^{n+1}) = \frac{1}{2}\int_{\Omega^{n+1}} \rho|\mathbf{u}^{n+1}|^2\mathrm{div}\,\mathbf{w}^n\,dx. \tag{34}$$

This term added to the last one of (33) exactly compensates for the quantity $-d^{n+1}(\mathbf{w}^n, \rho\mathbf{u}^{n+1}, \mathbf{u}^{n+1})$.

Finally, the third argument of the proof consists in noticing that the term coming from the Lorentz force $\frac{1}{\mu}l^{n+1}(\mathbf{u}^{n+1}, \mathbf{B}^n, \mathbf{B}^{n+1})$ exactly balances the coupling term in the magnetic equation. This fact comes from the way we linearize the equation in the Euler scheme (24).

Then, after some standard integrations by parts, we readily obtain (32). ♢

Remark 5.1 *The above result can be extended to the more realistic cases when* $\mathbf{f}$, $\mathbf{B}\cdot\mathbf{n}|_{\partial\Omega}$, $\mathbf{curl}\,\mathbf{B}\times\mathbf{n}|_{\partial\Omega}$ *are non zero. We skip this easy extension.*

6 Surface tension

Surface tension is a force appearing at the interface between the aluminium and the cryolite. This force tends to minimize the area of the interface. It is generally admitted that surface tension does not play a major role in aluminium electrolysis. Nevertheless, it might be not completely negligible, especially when physical instabilities appear. Moreover, it may also have a smoothing effect on the numerical instabilities of the interface. Therefore, it is useful to allow our computation to take it into account.

There is a large body of literature reporting on numerical results accounting for surface tension effects. However, to the best of our knowledge, not so much literature has been devoted to the detailed explanation of the numerical treatment of surface tension terms. In order to compensate for this lack and also for the sake of consistency, we now give the lines of our strategy, emphasying that we do not claim any originality. The reader familiar with this kind of problem may easily skip this part.

The classical Laplace formulation of the surface tension correlates the normal force with the main curvature of the surface (*see* L. Landau and E. Lifschitz [23] for example):

$$\mathrm{TS} = \gamma H \mathbf{n} \tag{35}$$

The parameter γ is the surface tension coefficient (in N/m) and H is the mean curvature positively counted with respect to the normal $\mathbf{n}$. The surface tension coefficient at the interface aluminium / cryolite is 0.5 N/m (in comparison of 0.07 N/m for water / air interface). In the non-dimensional formulation of Section 2.2, the following quantity must be added to the right-hand side of the equations:

$$\frac{1}{We}\tilde{H}\mathbf{n}$$

where $We = \rho_1 U^2 L/\gamma$ is the Weber number.

For a 1D surface (a curve) $H = \frac{1}{R}$, with R the radius of curvature positively counted along the normal. For a 2D surface, $H = \frac{1}{R1} + \frac{1}{R_2}$, with $R1$ and $R2$ the principal radiuses of curvature positively counted along the normal. The main difficulty to compute the surface tension is that it requires, at least in principle, the mean curvature of the surface, which is not trivial to evaluate on a discretized surface.

In order to discretize the surface tension, we multiply (35) by a test function Φ and integrate over the interface Σ :

$$\int_\Sigma \mathrm{TS}\Phi \, d\sigma = \int_\Sigma \gamma H \Phi.\mathbf{n} \, d\sigma \tag{36}$$

The mean curvature H can be expressed as the opposite of the trace of the derivative of the Gauss application which is the application associating to each point of the surface the normal of this surface. This can be written in the following way :

$$H = -\mathrm{tr}(\nabla_s \mathbf{n})$$

with ∇_s the gradient along the surface (more precisely, the orthogonal projection of the gradient onto the tangential space).

The generalization of the well-known divergence theorem to surfaces of non-zero curvature is the following:

$$\int_\Sigma \mathrm{tr}(\nabla_s \mathbf{n})\Phi.\mathbf{n} \, d\sigma = \int_\Sigma \mathrm{tr}(\nabla_s \Phi) \, d\sigma - \int_{\partial\Sigma} \Phi.\mathbf{m} \, dl. \tag{37}$$

The vector $\mathbf{m}$ is the normal vector to $\partial\Sigma$ (in the tangential space of Σ). The weak formulation of the surface tension is then :

$$\int_\Sigma \mathrm{TS}\Phi \, d\sigma = -\gamma \int_\Sigma \mathrm{tr}(\nabla_s \Phi) \, d\sigma + \gamma \int_{\partial\Sigma} \Phi.\mathbf{m} \, dl \tag{38}$$

The vector $\mathbf{m}$ is the contact angle between the interface and the wall, it is a data of the problem. In practice, we have chosen a contact angle equal to zero. We now have to express the derivative $\mathrm{tr}(\nabla_s \Phi)$ on the discretized surface Σ.

In one dimension, it is easy to evaluate $\mathrm{tr}(\nabla_s \Phi)$ using the formula :

$$\mathrm{tr}(\nabla_s \Phi) = \frac{< d\Phi(e_u), e_u >}{||e_u||^2}$$

with $d\Phi(e_u) = \frac{d\Phi}{du}$. In this formula, e_u is a vector in the tangent space : $e_u = \frac{\partial f}{\partial u}$ with f a parameterization of the curve. In practice, this parameterization is given by the application which sends the element of reference $[0,1]$ onto the finite element. The derivative $\frac{d\Phi}{du}$ is then evaluated by finite differences. We are now going to generalize this approach in two dimensions.

In order to evaluate the divergence along the surface $\mathrm{tr}(\nabla_s \Phi)$ in two dimensions, we need a local parameterization $f : U \subset \mathbb{R}^2 \to \mathbb{R}^3$. From a discrete point of view, this parameterization is given by the finite element test functions (we suppose that we use Lagrangian finite element) :

$$f : \left\{ \begin{array}{ccc} [0,1]^2 & \to & \mathbb{R}^3 \\ (u,v) & \mapsto & \displaystyle\sum_{P \in \mathcal{P}(\mathcal{E})} \phi_P X_P \end{array} \right.$$

where $\phi_P : [0,1]^2 \to \mathbb{R}$ is the shape function related to the point P, X_P is the coordinate vector of P and $\mathcal{P}(\mathcal{E})$ is the set of the points of the element $\mathcal{E}$. A basis of the tangential space is given by (e_u, e_v) with $e_u = \frac{\partial f}{\partial u}$ and $e_v = \frac{\partial f}{\partial v}$. The metric tensor M is the matrix $\begin{bmatrix} E & F \\ F & G \end{bmatrix}$ with $E = ||e_u||^2$, $F =< e_u, e_v >$ and $G = ||e_v||^2$. The element of area is $da = \sqrt{EG - F^2}\, du\, dv$. We want to evaluate the trace of the derivative $d\Phi$ along the surface. We define : $e =< d\Phi(e_u), e_u >$, $f_1 =< d\Phi(e_u), e_v >$, $f_2 =< d\Phi(e_v), e_u >$ and $g =< d\Phi(e_v), e_v >$. Of course, we have $d\Phi(e_u) = \frac{\partial \Phi}{\partial u}$ and $d\Phi(e_v) = \frac{\partial \Phi}{\partial v}$. We have the following equality :

$$\begin{bmatrix} e & f_1 \\ f_2 & g \end{bmatrix} = \begin{bmatrix} a_{1,1} & a_{1,2} \\ a_{2,1} & a_{2,2} \end{bmatrix} \begin{bmatrix} E & F \\ F & G \end{bmatrix}$$

with $A = [a_{i,j}]$ the matrix of the derivative $d\Phi$ in the basis (e_u, e_v). A simple computation gives the following expression of $H = -(a_{1,1} + a_{2,2})$:

$$H = -\frac{eG + Eg - F(f_1 + f_2)}{EG - F^2}$$

Let us now explain the way we evaluate e, $f1$, $f2$ and g for a $Q1$ discretization (see figure

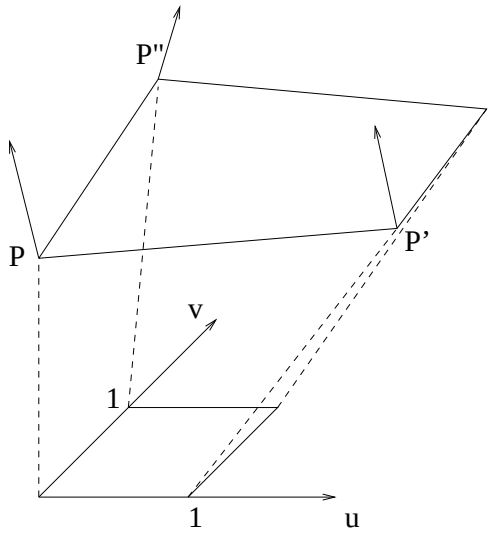

Figure 3: A $Q1$ element parameterized by $[0,1]^2$.

3). Let P be the point $(0,0)$, P', the point $(1,0)$ and P'' the point $(0,1)$. The application

$f_0(t) = f(t,0)$ is a parameterization of $[PP']$. Then, we have :

$$\begin{aligned} d\Phi(P)(e_u) &= \frac{d}{dt}(\Phi(\gamma(t))|_{t=0} \\ &\sim \Phi(\gamma(1)) - \Phi(\gamma(0)) \\ &\sim \Phi(P') - \Phi(P) \end{aligned}$$

In the same manner, we derive :

$$d\Phi(P)(e_v) \sim \Phi(P'') - \Phi(P)$$

and therefore :

$$\begin{aligned} e &\sim < \Phi(P') - \Phi(P), e_u > \\ f_1 &\sim < \Phi(P') - \Phi(P), e_v > \\ f_2 &\sim < \Phi(P'') - \Phi(P), e_u > \\ g &\sim < \Phi(P'') - \Phi(P), e_v > \end{aligned}$$

We can therefore evaluate the mean curvature H, using finite difference approximations.

7 Numerical experiments

All the results shown in this section are presented in the non-dimensional form detailed in Section 2.2.

7.1 On the mass conservation

We described precisely in Section 5.2 the three key arguments that allow us to ensure mass conservation in the two-fluid problems. We give in this section a few illustrations of mass loss if some of the requirements are not fulfilled.

For this purpose, we consider the case when the two fluids are only subjected to an oscillating gravity. The computational domain is $\Omega = [-2,2] \times [0,2]$, the lower (resp. upper) fluid occupies at $t = 0$ the subdomain $\Omega_{1,t=0} = [-2,2] \times [0,1]$ (resp. $\Omega_{2,t=0} = [-2,2] \times [1,2]$). The potential of the body force is given by:

$$\tilde{\Phi}(x,y,t) = Ax \sin(2\pi\nu t) - y$$

We choose the following non-dimensional parameters: $Re_1 = Re_2 = 100$, $M = 0.91$, $\nu = 0.0625$, $A = 0.05$. Figure 4 shows the evolution in time of the elevation of a point on the interface.

In Figure 5, we show the evolution in time of the mass of fluid 1 with three finite element spaces: Q2/Q1 (with a continuous pressure), Q2/P1 (with a discontionuous pressure), and

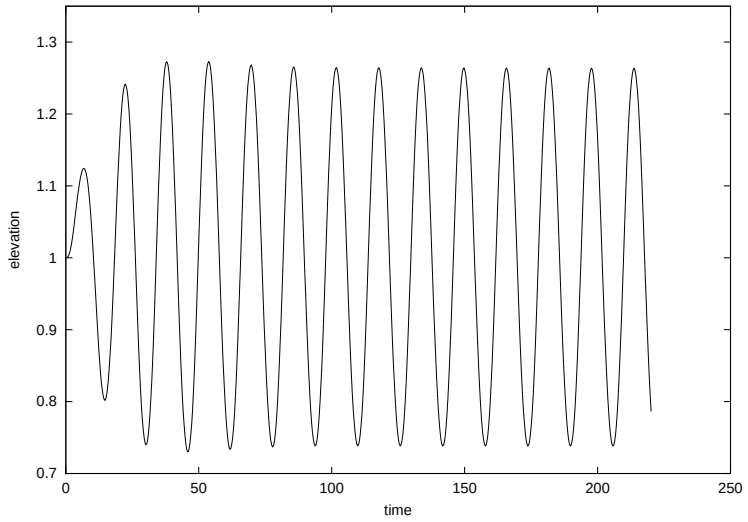

Figure 4: The time history of the elevation of a point of the interface.

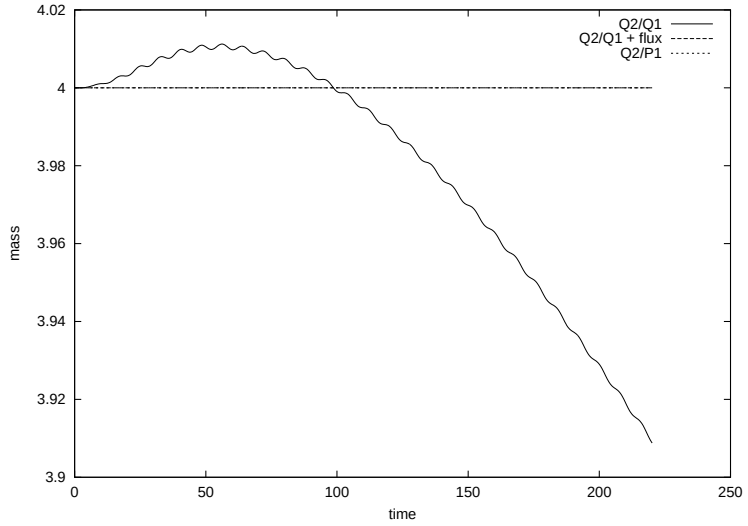

Figure 5: Mass conservation is ensured with Q2/P1 or Q2/Q1 with a flux constraint (the two curves are the same), but it fails with Q2/Q1 elements.

Q2/Q1 with the flux constraint (31). The pair Q2/Q1 does not satisfy (30) which explains the non conservation of mass.

We now illustrate the role of the GCL in mass conservation. We use the Q1/Q1 stabilized finite element with flux constraint (31). Thus)29) is now satisfied. If the displacement of the mesh is purely vertical, the GCL property (26) is satisfied, and the mass is preserved. But, if we replace system (25) by

$$\begin{cases} -\triangle \mathbf{w} = 0, & \text{on } \Omega_i^n, \\ \mathbf{w} = \mathbf{u}, & \text{on } \Sigma^n, \\ \dfrac{\partial \mathbf{w}}{\partial n} = 0 & \text{on } \partial\Omega, \end{cases} \tag{39}$$

the displacement of the mesh is now arbitrary, and relation(26) is no more true. We show on the left-hand side of Figure 6, the mesh obtained with (25) and on the right-hand side, the one obtained with (39). Of course, it seems not very natural to allow for a mesh displacement along to x axis for this test case, but it is just for illustration. We see on Figure 7 that the mass is not preserved when the displacement is along x and y. The fact that relation (30) is not sufficient on a moving mesh to ensure mass conservation is striking.

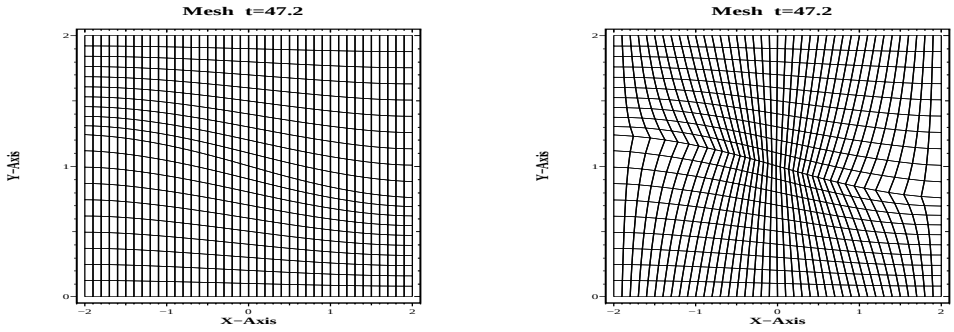

Figure 6: The velocity of the mesh is computed with (25) on the left-hand side, and with (39) on the right-hand side.

7.2 A MHD experiment with a free surface and a free interface

We present here the numerical simulation of a laboratory MHD experiment (described by R. Moreau [27, 28]). A uniform vertical electrical current flows in a cylindrical tank through two layers of fluid subjected to the gravity. The interface between the fluid and the upper surface are both free (see Figure 8). The above formulation must be slightly modified to treat this case due to the presence of two free surfaces, but the modifications are straightforward and we do not detail them here. Let us just mention that, because of the presence of the upper free surface, we do not perform the "pressure correction" presented in Section 2.2.

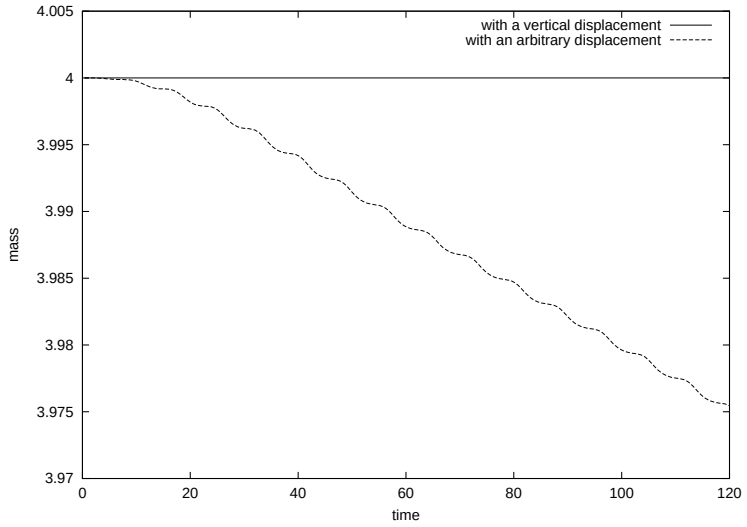

Figure 7: Both curves are obtained with Q1/Q1 finite element with flux constraint (31). When the displacement of the mesh is arbitrary, Lemma 1 does not apply and we observe a mass loss, contrarily to the case when the displacement is purely vertical.

This test case is of interest for two reasons: first, the physical system is not too far from the aluminium electrolysis, and second, an analytical steady state solution is known.

We denote by $\tilde{J}_0$ the intensity of the non-dimensional homogeneous density of current and by R the radius of the cylinder. Working with the natural cylindrical coordinates $(\mathbf{e}_r, \mathbf{e}_\theta, \mathbf{e}_z)$ associated with the cylindrical tank, we have:

$$\tilde{\mathbf{B}} = \tilde{B}(r)\mathbf{e}_\theta, \qquad \text{with } \tilde{B}(r) = -\frac{J_0}{2}r \quad (\text{for } r \leq R),$$

and the magnetic force is

$$S\,\mathbf{curl}\,\tilde{\mathbf{B}} \times \tilde{\mathbf{B}} = -\frac{SJ_0^2}{2} r\,\mathbf{e}_r.$$

The only body force being the gravity, we have $\tilde{\Phi} = -z$. Looking for a solution with $\mathbf{u} = 0$, we have

$$\nabla\tilde{p} = -\frac{m}{Fr}\mathbf{e}_z - \frac{SJ_0^2}{2} r\,\mathbf{e}_r, \tag{40}$$

with $m = M$ in the upper fluid and $m = 1$ in the lower one. Thus

$$\tilde{p}(r,z) = -\frac{m}{Fr}z - \frac{SJ_0^2}{4}r^2 + C,$$

where C is a constant. We denote by h_1^0 (resp. h_2^0) the elevation of the free interface (resp. surface) before the application of the electrical current, and by $h_1(r)$ (resp. $h_2(r)$) their steady state elevation, in the presence of the electrical current. The pressure above the free surface is supposed to be constant and equal to zero. Thus, we have:

$$0 = \tilde{p}(r, h_2(r)) = -\frac{M}{Fr} h_2(r) - \frac{S J_0^2}{4} r^2 + C$$

The constant C is then determined by writing the conservation of the volume of the upper fluid, and we finally obtain:

$$h_2(r) = h_2^0 + \frac{S\, Fr\, J_0^2 R^2}{8M} \left(1 - \frac{2r^2}{R^2}\right) \tag{41}$$

Next, taking the **curl** of equation (40), we have:

$$0 = \mathbf{curl}\left(\frac{m}{Fr}\mathbf{e}_z\right) = \nabla\left(\frac{m}{Fr}\right) \times \mathbf{e}_z = \frac{M-1}{Fr}\mathbf{n} \times \mathbf{e}_z,$$

where $\mathbf{n}$ is the normal to the interface. Therefore, $\mathbf{n} = \mathbf{e}_z$, which proves that the steady state interface is horizontal:

$$h_1(r) = h_1^0.$$

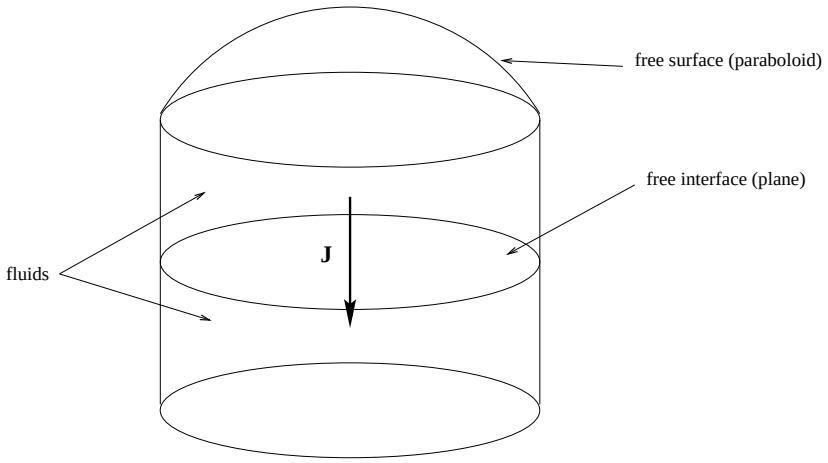

Figure 8: Schematic representation of the experiment of Section 7.2.

We use the following numerical values: $Re_1 = Re_2 = 200$, $S = 1$, $Rm_1 = Rm_2 = 1$, $Fr = 8$, $J_0 = 0.3$, $M = 0.5$, $We = 10^2$. Figure 9 shows a comparison between the elevation

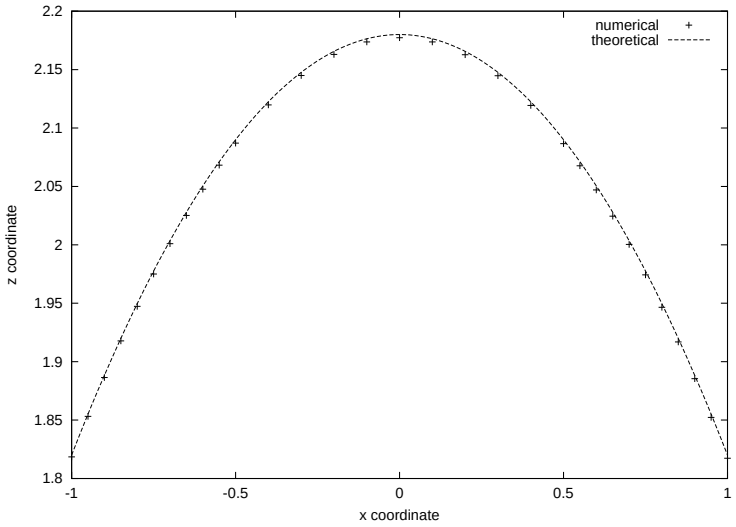

Figure 9: Elevation of the steady state top surface in the simulation of Section 7.2. Comparison between theoretical and numerical results.

of the upper surface and the analytical solution (41) along the plane $y = 0$. Figure 10 shows the steady-state upper surface and the interface. Figure 11 shows the time evolution of the elevation of the center of the upper surface (left-hand side) and of the interface (right-hand side).

7.3 Metal pad roll instabilities

One of the phenomena which is observed in industrial cells and which has been a lot investigated over the past few years is metal pad rolling. It is an oscillation of the cryolite / aluminium interface with a period ranging from five seconds up to more than one minute. The aim of most of the theoretical and experimental studies of MHD cells has been to understand, forecast and avoid this phenomenon. See A.F. LaCamera, D.P. Ziegler and R.L. Kozarek [22] and the references herein for a survey on the main approaches until 1992.

One of the explanation of the metal pad rolling is the presence of a vertical field. The famous Sele's criterion belongs to this theory (cf. T. Sele [34]). T. Sele has been the first one to give a physical reason of the rotation by the interaction of the vertical magnetic field with horizontal perturbed currents. More recently, P.A. Davidson and R.I. Lindsay [3] have derived a more general linearized system. Their analysis leads to quantitative results for the instability of standing and travelling waves in rectangular and circular cells. They also give a mechanical analogue which provides a good physical insight into the phenomenon.

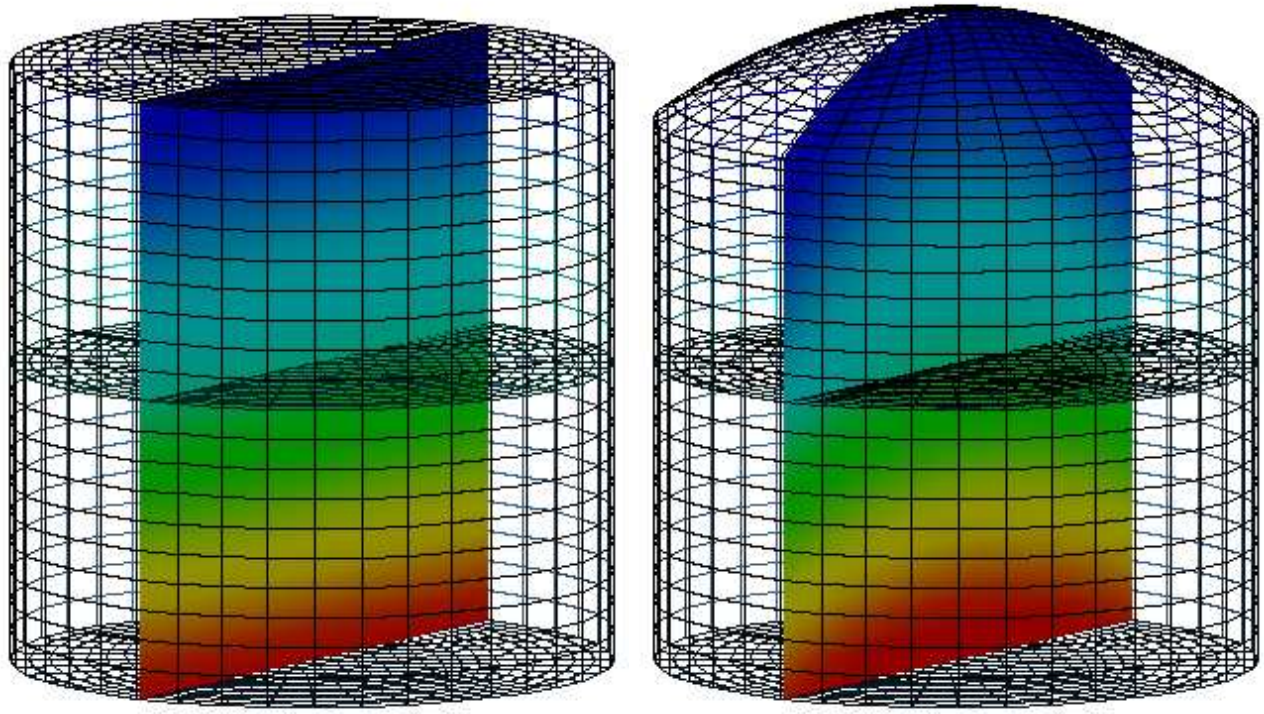

Figure 10: Mesh and Isovalues of pressure on a portion of the mesh, in presence of gravity (left), after the application of an electrical current (right)

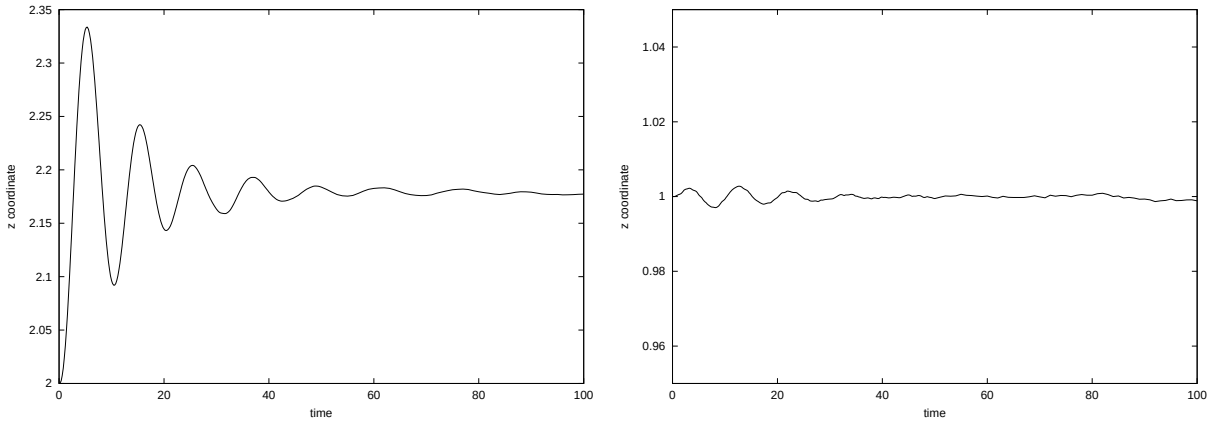

Figure 11: Evolution in time of the elevation of centers of the top surface (left) and of the interface (right) in the simulation of Section 7.2.

The physical phenomenon is explained on Figure 12. An initial tilting (or a long-wavelength disturbance) creates a perturbed current flow $\mathbf{j} = \mathbf{J} - \mathbf{J_0}$ ($\mathbf{J_0}$ denotes the unperturbed – or background – current and $\mathbf{J}$ the total current in the cell) which is mainly vertical in the cryolite and horizontal in the aluminium (because of the strong difference of electrical conductivity). The interaction of this current with the vertical magnetic field results in a horizontal Lorentz force $\mathbf{F} = \mathbf{j} \times \mathbf{B}$, in the direction perpendicular to $\mathbf{j}$. It consequently induces a rotating motion of the interface.

In some cases, this phenomenon can lead to an instability: when the vertical field is too large, the amplitude of the oscillation may grow with time. It has been reported on that the metal can even get out of the cell in some cases !

In [3], it is shown that it is the interaction between gravitational modes which leads to instable rolling waves. In particular, the authors assert that a circular cell becomes instable whenever a vertical field B_z is applied. We have chosen to reproduce this simple experiment of a circular cell to check this strong result of instability, which is obtained after many assumptions and linearization (cf. [3]). The linearized approach may well reproduced qualitatively the metal pad rolling, but a few of the assumptions are quite questionable as far as quantitative results are concerned.

The test case cell is a circular cell of radius equals to 1 and height equals to 2. Initially, the fluids are at rest, the interface is situated at the mean height and is flat and horizontal. On the wall, we impose during the whole simulation the magnetic boundary conditions corresponding to a uniform vertical electrical current $J_0\mathbf{e}_z$ (when the fluids are at rest and the interface is horizontal). For $0 \leq t \leq 1$, the fluids are subjected to a gravity having an angle of 5 degree with the vertical. This slightly "tilts" the cell and creates an initial disturbance. For $1 < t \leq 25$, the gravity is put straight again, and a vertical magnetic field B_z is superimposed to the magnetic field created by the electrical current. This actually

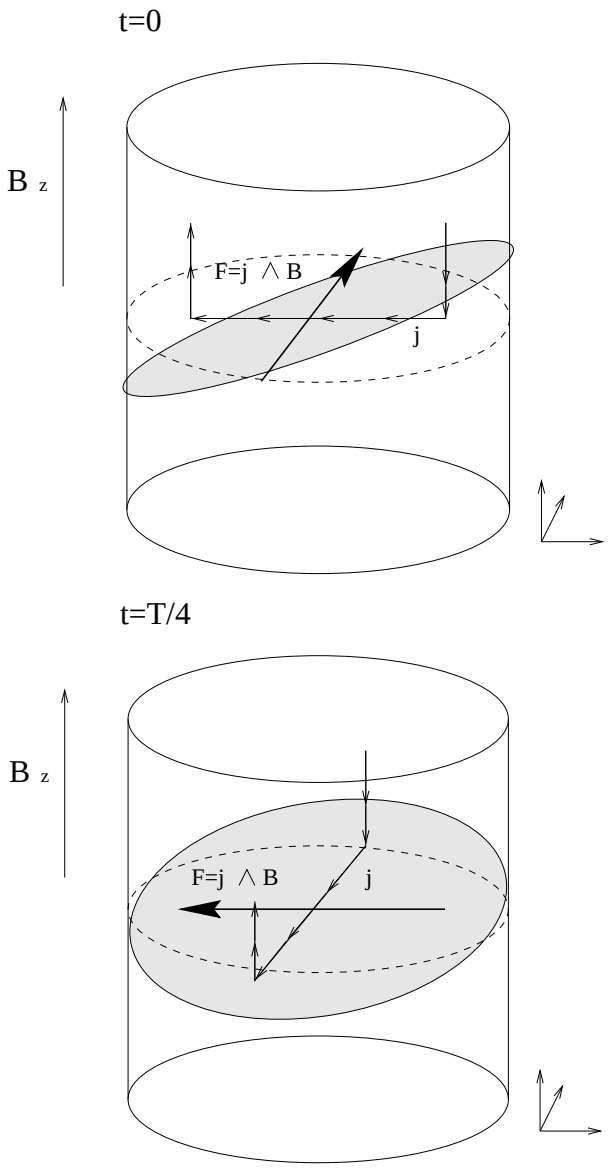

Figure 12: Rolling phenomenon.

induces the metal rolling phenomenon. For $t > 25$, the vertical magnetic field is removed, and the system can therefore retrieve its initial configuration, at least when it does not explode before. The non-dimensional parameters are the following: $Re_1 = Re_2 = 1000$, $M = 0.935$, $Fr = 0.1$, $Rm_1 = 10^{-4}$, $Rm_2 = 1.$, $S = 1.$, $We = 50$, $J_0 = 2$. We perform the simulations for various values of B_z. Figure 13 shows the lower fluid and the interface when $B_z = 0.2$. Figure 14 shows the evolution in time of the elevation of the point of the interface initially situated at $(1., 0., 1.)$ for $B_z = 0.1, 0.2, 0.3$ and 0.5. The three last values lead to an "explosion" of the interface. The physical explanation of the phenomenon proposed on Figure 12 can be checked by computing the disturbed currents. In order to compute this disturbance, the initial current $\mathbf{curl}\,\mathbf{B}_0$ is substracted from $\mathbf{curl}\,\mathbf{B}$. A few streamlines of the perturbated current are represented on Figure 15: there is indeed a "loop of current" as predicted in the theoretical explanation of the phenomenon.

In other simulations, we have also observed that small disturbances of the initial state do not lead to instability, at least on a reasonable time scale. In the same way, a small positive B_z does not induce instability. This is in apparent contradiction with the results of the linear approach which claim the instability of the cell. At least our results show that, should the instability occur, it will occur only in the large time limit, and therefore may not be relevant from the practical viewpoint. Of course, definite conclusions about this comparison between the two approaches are yet to be obtained.

This test case demonstrates the capability of our nonlinear approach to simulate complex MHD phenomena. In the past, these phenomena were analyzed with models based on many simplifications of the original equations providing excellent qualitative results most of the time. But the influences of such simplifications need in any case to be tested and may become not negligible when precise results are desired. We have demonstrated that we can reproduce qualitatively the results predicted by simplified models, but that we are also able to give *quantitative* informations on the transient evolution of the system. This capability should have practical implications in the study of the instabilities of industrial cells.

Acknowledgements. We thank B. Maury (Université Paris 6) for his help and advice and N. Ligonesche (Pechiney) for stimulating discussions. This work was partially supported by Aluminium Pechiney, LRF.

References

[1] T.A. Baer, R.A. Cairncross, P.R. Schunk, P.A. Sackinger, and R.R. Rao. A finite element method for free surface flows of incompressible fluids in three dimensions. Part II: dynamic wetting line. *Int. Jour. Num. Meth. Fluids*, 33:405–427, 2000.

[2] R.A. Cairncross, P.R. Schunk, T.A. Baer, R. Rao, and P.A. Sackinger. A finite element method for free surface flows of incompressible fluids in three dimensions. Part I: Boundary fitted mesh motion. *Int. Jour. Num. Meth. Fluids*, 33:375–403, 2000.

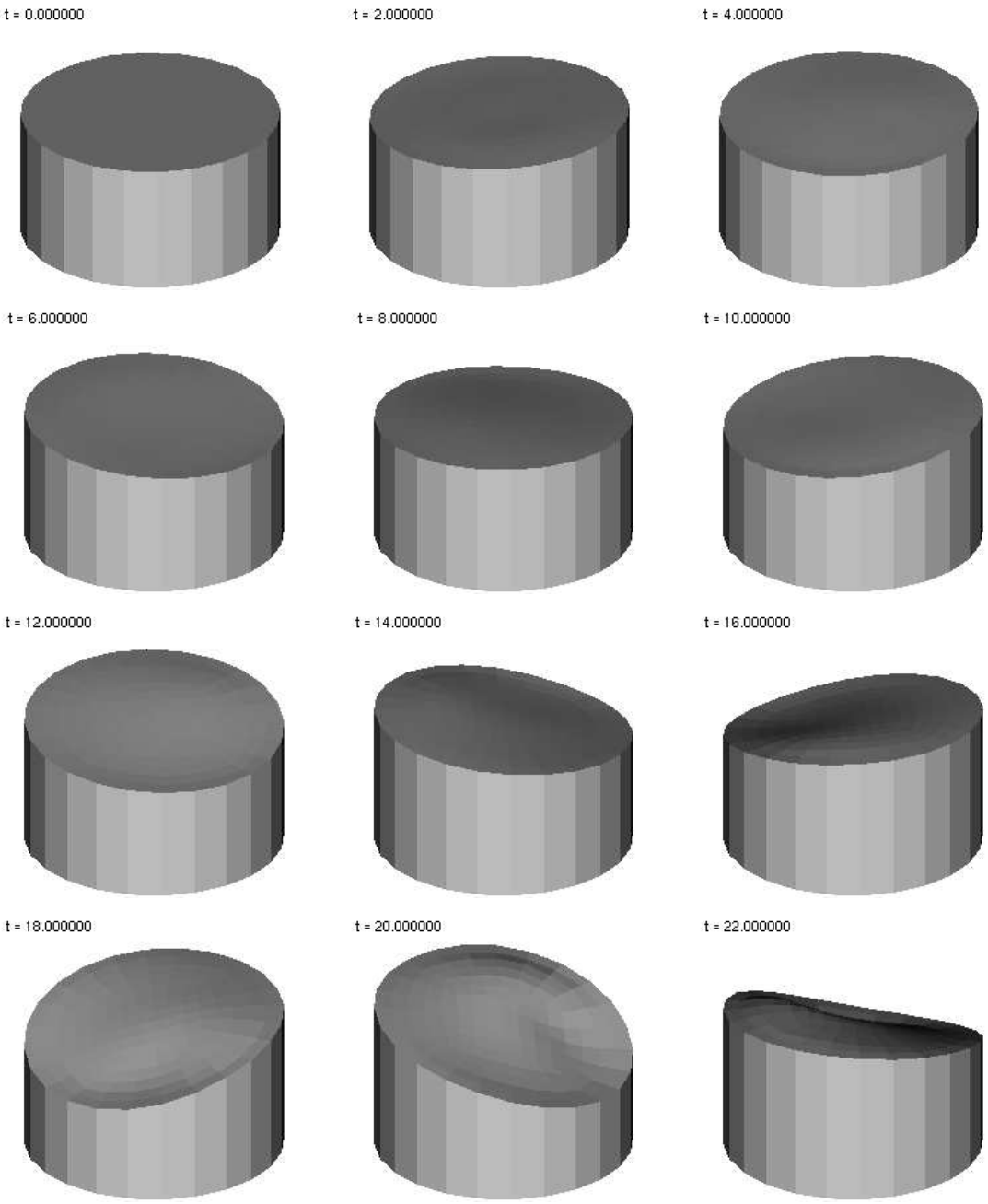

Figure 13: The phenomenon of metal pad rolling in a circular cell. Visualization of the interface and the lower fluid (the upper fluid is not represented for the sake of clarity). This is a case with $B_z = 0.2$.

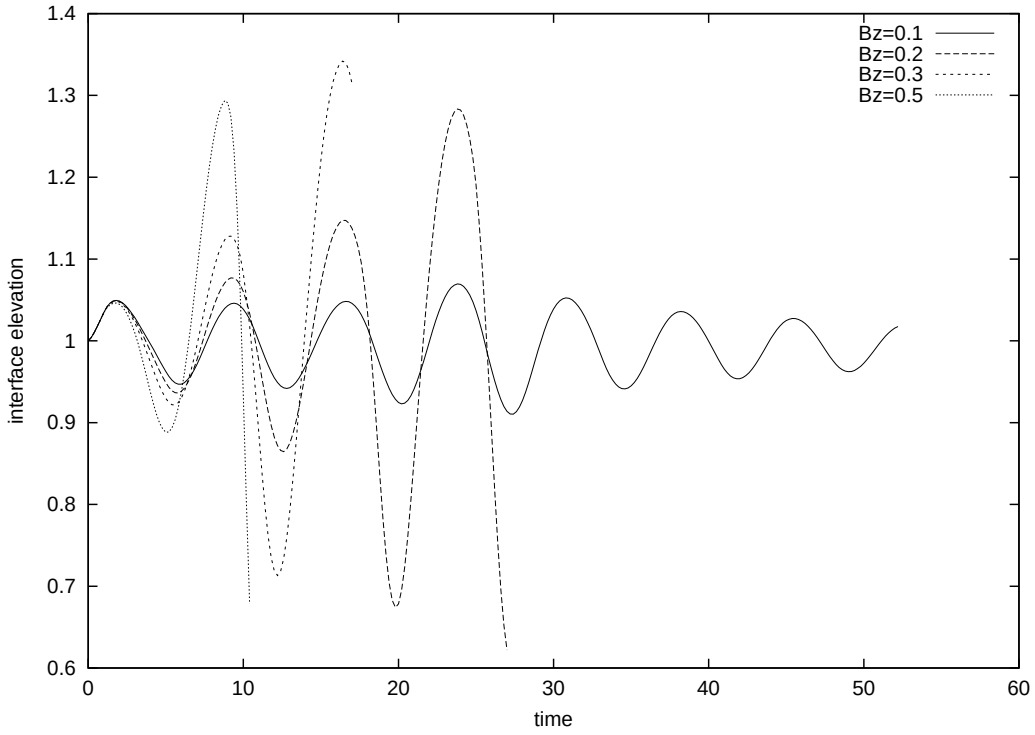

Figure 14: Time evolution of the elevation of a point of the interface in the "metal pad roll" experiment for various values of B_z. The only stable simulation is obtained with $B_z = 0.1$.

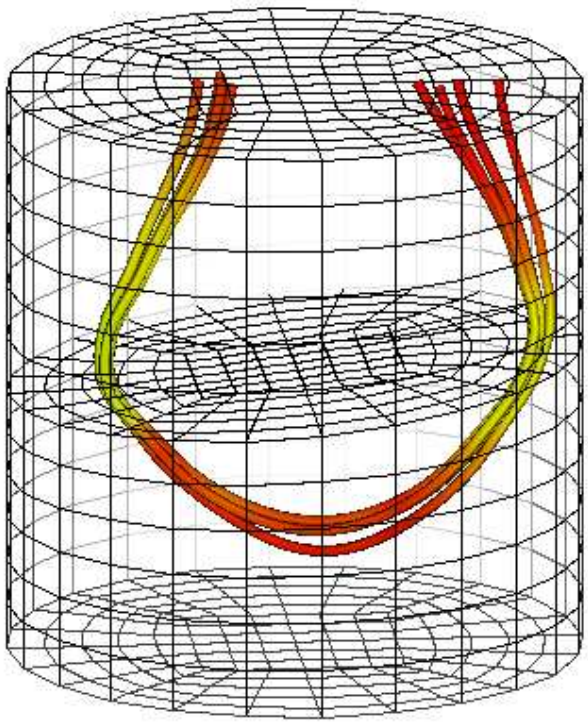

Figure 15: Loops of currents in cryolite during metal pad roll. We show here some streamlines of the field $\mathbf{j}$ (the perturbed current). The perturbed current goes here from the right-hand side of the Figure (where the elevation of the interface is the highest) to the left-hand side.

[3] P.A Davidson and R.I. Lindsay. Stability of interfacial waves in aluminium reduction cells. *J. Fluid Mech.*, 362:273–295, 1998.

[4] J. Descloux, M. Flueck, and M.V. Romerio. Modelling for instabilities in hall-heroult cells : mathematical and numerical aspects. *Magnetohydrodynamics in Process Metallurgy*, pages 107–110, 1991.

[5] J. Descloux, M. Flueck, and M.V. Romerio. Stability in aluminium reduction cells : a spectral problem solved by an iterative procedure. *Light Metal*, pages 275–281, 1994.

[6] L. Formaggia, J.-F. Gerbeau, F. Nobile, and A. Quarteroni. Numerical treatment of defective boundary conditions for the navier-stokes equations. Research Report RR-4093, INRIA, 2001.

[7] L. Formaggia and F. Nobile. A stability analysis for the arbitrary Lagrangian Eulerian formulation with finite elements. *East-West J. Numer. Math.*, 7(2):105–131, 1999.

[8] J.-F. Gerbeau. Comparison of numerical methods for solving a magnetostatic problem. application to the magnetohydrodynamic equations. In *Proceedings of the Fourth European Computational Fluid Dynamics, ECCOMAS 98*, pages 821–825. Wiley, 1998.

[9] J.-F. Gerbeau. A stabilized finite element method for the incompressible magnetohydrodynamic equations. *Numerische Mathematik*, 87(1):83–111, 2000.

[10] J.-F. Gerbeau and C. Le Bris. Existence of solution for a density-dependent magnetohydrodynamic equation. *Advances in Differential Equations*, 2(3):427–452, May 1997.

[11] J.-F. Gerbeau and C. Le Bris. On a coupled system arising in magnetohydrodynamics. *Appl. Math. Lett.*, 12:53–57, 1999.

[12] J.-F. Gerbeau and C. Le Bris. On the long time behaviour of the solution to the two-fluids incompressible navier-stokes equations. *Differential Integral Equations*, 12(5):691–740, 1999.

[13] J.-F. Gerbeau and C. Le Bris. Comparison between two numerical methods for a magnetostatic problem. *Calcolo*, 37(1):1–20, 2000.

[14] J.-F. Gerbeau, C. Le Bris, and M. Bercovier. Spurious velocities in the steady flow of an incompressible fluid subjected to external forces. *Int. Jour. Num. Meth. Fluids*, 25:679–695, October 1997.

[15] J.-F. Gerbeau, T. Lelievre, C. Le Bris, and N. Ligonesche. Metal pad roll instabilities. *Light Metal*, 2002. to appear.

[16] R. Glowinski, P. Le Tallec, M. Ravachol, and V. Tsikkinis. Numerical solution of the Navier-Stokes equations modeling the flow of two incompressible nonmiscible viscous fluids. In *Finite elements in fluids, Vol. 8 (Huntsville, AL, 1989)*, pages 137–163. Hemisphere, Washington, DC, 1992.

[17] H. Guillard and C. Farhat. On the significance of the geometric conservation law for flow computations on moving meshes. *Comput. Methods Appl. Mech. Engrg.*, 190(11-12):1467–1482, 2000.

[18] M.D. Gunzburger, A.J. Meir, and J.S. Peterson. On the existence, uniqueness, and finite element approximation of solutions of the equations of stationary, incompressible magnetohydrodynamics. *Mathematics of Computation*, 56(194):523–563, April 1991.

[19] L.W. Ho. *A legendre spectral element method for simulation of incompressible unsteady viscous free-surface flows.* PhD thesis, Massachussets Institute of Technology, 1989.

[20] A. Huerta and W. K. Liu. Viscous flow with large surface motion. *Comp. Meth. Appl. Mech. Engng.*, 69:277–324, 1988.

[21] W.F. Hughes and F.J. Young. *The electromagnetodynamics of fluids.* Wiley, 1966.

[22] A.F. LaCamera, D.P. Ziegler, and R.L. Kozarek. Magnetohydrodynamics in the Hall-Héroult process, an overview. *Light Metals*, pages 1179–1186, 1992.

[23] L. Landau and E. Lifchitz. *Course of Theoretical Physics, volume 6.* Pergamon Press, 1984.

[24] P. Le Tallec and J. Mouro. Fluid structure interaction with large structural displacements. *Comput. Meth. Appl. Mech. Engrg.*, 190:3039–3067, 2001.

[25] M. Lesoinne and C. Farhat. Geometric conservation laws for flow problems with moving boundaries and deformable meshes and their impact on aeroelastic computations. *Computer Methods in Applied Mechanics and Engineering*, 134:71–90, 1996.

[26] B. Maury. Characteristics ALE methods for the unsteady 3D Navier-Stokes equations with a free surface. *Comp. Fluid. Dyn.*, 6:175–188, 1996.

[27] R. Moreau. *Magnetohydrodynamics.* Kluwer Academic Publishers, 1990.

[28] R. Moreau. Ecoulement d'un métal liquide en présence d'un champ magnétique. In *Traité de Génie électrique*, volume D4, pages D2950–3 – D2950–30. Editions Techniques de l'ingénieur, 1992.

[29] R. Moreau and J.W. Evans. An analysis of the hydrodynamics of aluminium in reduction cells. *J. Electrochem. Soc.: Electrochem. Sci. Tech.*, 131(10):2251–2259, 1984.

[30] R. Moreau and D. Ziegler. The moreau-evans hydrodynamic model applied to actual hall-héroult cells. *Metal. Trans. B.*, 19B:737–744, 1988.

[31] B. Nkonga and H. Guillard. Godunov type method on nonstructured meshes for three-dimensional moving boundary problems. *Comput. Methods Appl. Mech. Engrg.*, 113(1-2):183–204, 1994.

[32] H.K. Rasmussen, O. Hassager, and A. Saasen. Viscous flow with large fluid-fluid interface displacement. *Int. Jour. Num. Meth. Fluids*, 28:859–881, 1998.

[33] M. Segatz and C. Droste. Analysis of magnetohydrodynamic instabilities in aluminium reduction cells. *Light Metals*, pages 313–322, 1994.

[34] T. Sele. Instabilities of the metal surface in electrolytic cells. *Light Metal*, pages 7–24, 1977.

[35] A.D. Sneyd and A. Wang. Interfacial instability due to mhd mode coupling in aluminium reduction cells. *J. Fluid Mech.*, 263:343–359, 1994.

[36] A. Soulaïmani, M. Fortin, G. Dhatt, and Y. Ouellet. Finite element simulation of two- and three dimensional free surface flows. *Comp. Meth. Appl. Mech. Engng*, 86:265–296, 1991.

[37] A. Soulaïmani and Y. Saad. An arbitrary Lagrangian-Eulerian finite element method for solving three-dimensional free surface flows. *Comput. Meth Appl. Mech Engrg.*, 162:79–106, 1998.

Unité de recherche INRIA Rocquencourt
Domaine de Voluceau - Rocquencourt - BP 105 - 78153 Le Chesnay Cedex (France)

Unité de recherche INRIA Lorraine : LORIA, Technopôle de Nancy-Brabois - Campus scientifique
615, rue du Jardin Botanique - BP 101 - 54602 Villers-lès-Nancy Cedex (France)
Unité de recherche INRIA Rennes : IRISA, Campus universitaire de Beaulieu - 35042 Rennes Cedex (France)
Unité de recherche INRIA Rhône-Alpes : 655, avenue de l'Europe - 38330 Montbonnot-St-Martin (France)
Unité de recherche INRIA Sophia Antipolis : 2004, route des Lucioles - BP 93 - 06902 Sophia Antipolis Cedex (France)

Éditeur
INRIA - Domaine de Voluceau - Rocquencourt, BP 105 - 78153 Le Chesnay Cedex (France)
http://www.inria.fr
ISSN 0249-6399